REPORT DOCUMENTATION PAGE

1a. REPORT SECURITY CLASSIFICATION Unclassified	1b. RESTRICTIVE MARKINGS
2a. SECURITY CLASSIFICATION AUTHORITY	3. DISTRIBUTION / AVAILABILITY OF REPORT
2b. DECLASSIFICATION / DOWNGRADING SCHEDULE	Approved for public release; distribution unlimited.

DTIC ELECTE FEB27 1990 S B D

4. PERFORMING ORGANIZATION REPORT NUMBER(S)	5. MONITORING ORGANIZATION REPORT NUMBER(S) ARO 23004.4-PH-A

6a. NAME OF PERFORMING ORGANIZATION Honeywell Inc.	6b. OFFICE SYMBOL (If applicable)	7a. NAME OF MONITORING ORGANIZATION U. S. Army Research Office

6c. ADDRESS (City, State, and ZIP Code) Bloomington, Minnesota 55420	7b. ADDRESS (City, State, and ZIP Code) P. O. Box 12211 Research Triangle Park, NC 27709-2211

8a. NAME OF FUNDING / SPONSORING ORGANIZATION U. S. Army Research Office	8b. OFFICE SYMBOL (If applicable)	9. PROCUREMENT INSTRUMENT IDENTIFICATION NUMBER DAAG29-85-C-0028

8c. ADDRESS (City, State, and ZIP Code) P. O. Box 12211 Research Triangle Park, NC 27709-2211	10. SOURCE OF FUNDING NUMBERS

PROGRAM ELEMENT NO.	PROJECT NO.	TASK NO.	WORK UNIT ACCESSION NO.

11. TITLE (Include Security Classification)

Nonlinear Optical Effects in GaAs/AlGaAs Superlattices

12. PERSONAL AUTHOR(S)
John A. Lehman

13a. TYPE OF REPORT Final	13b. TIME COVERED FROM 10/1/85 TO 9/30/89	14. DATE OF REPORT (Year, Month, Day) Nov 15, 89	15. PAGE COUNT 63

16. SUPPLEMENTARY NOTATION The view, opinions and/or findings contained in this report are those of the author(s) and should not be construed as an official Department of the Army position, policy, or decision, unless so designated by other documentation.

17.	COSATI CODES		18. SUBJECT TERMS (Continue on reverse if necessary and identify by block number)
FIELD	GROUP	SUB-GROUP	Superlattices, Gallium Arsenide Superlattices,
			Nonlinear Optical Effects, Compositional Superlattices,
			Superlattice Optical Behavior

19. ABSTRACT (Continue on reverse if necessary and identify by block number)

The main purpose of this program was to thoroughly study the nature of the optical nonlinearities demonstrated in GaAs superlattices and show potential for device applications. The nonlinear properties in three main types of superlattices were investigated; GaAs/AlGaAs compositional superlattices, GaAs doping superlattices and GaAs/AlGaAs Hetero-nipi superlattices (Figure 1.0.1). Compositional superlattices were studied because theoretical work done in the area of nonlinear optical effects in multiple quantum wells (compositional superlattices) in GaAs/AlGaAs had evidence to show that due to the special properties of a superlattice, a 100X enhancement in the

(Continued on reverse side)

20. DISTRIBUTION / AVAILABILITY OF ABSTRACT ☐ UNCLASSIFIED/UNLIMITED ☐ SAME AS RPT. ☐ DTIC USERS	21. ABSTRACT SECURITY CLASSIFICATION Unclassified
22a. NAME OF RESPONSIBLE INDIVIDUAL	22b. TELEPHONE (Include Area Code)	22c. OFFICE SYMBOL

AD-A218 543

nonlinearity should be expected over that of bulk GaAs. In particular the dependence of the nonlinearity on the well thickness was studied both experimentally and theoretically. GaAs doping superlattices were investigated because it was believed that large nonlinearities could be induced at very low powers due to the tuneable carrier lifetime. The dependence of the nonlinearity on the power was studied. GaAs/AlGaAs Hetero-nipis were studied as an extention of GaAs doping superlattices.

The nonlinear effects in the three types of superlattices were explored by 1) growing high quality material by MOCVD and MBE, 2) characterizing the nonlinear optical properties using various experimental techniques, and 3) developing theoretical models which predict the superlattice optical behavior.

The nonlinear effects in the three types of superlattices were explored by 1) growing high quality material by MOCVD and MBE, 2) characterizing the nonlinear optical properties using various experimental techniques, and 3) developing theoretical models which predict the superlattice optical behavior.

NONLINEAR OPTICAL EFFECTS IN

GaAs/AlGaAs SUPERLATTICES

Final Report

prepared by:

Mr. John A. Lehman
Research Scientist
Systems and Research Center
Honeywell Inc.

November 15, 1989
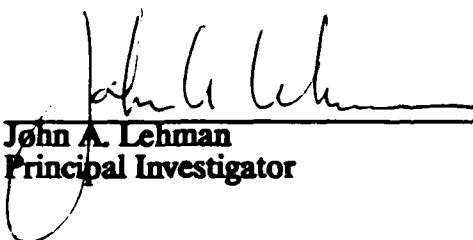
for:

U. S. ARMY RESEARCH OFFICE

Contract #:
DAAG29-85-C-0028

90 02 26 035

NONLINEAR OPTICAL EFFECTS IN

GaAs/AlGaAs SUPERLATTICES

Final Report

prepared by:

Mr. John A. Lehman
Research Scientist
Systems and Research Center
Honeywell Inc.

November 15, 1989

for:

U. S. ARMY RESEARCH OFFICE
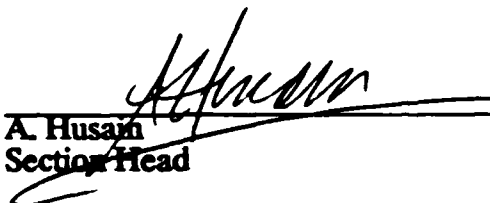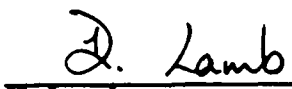
Contract #:
DAAG29-85-C-0028

NONLINEAR OPTICAL EFFECTS IN GaAs/AlGaAa SUPERLATTICES PROGRAM

Final Report

1 October 1985 to 30 September 1989

Date: 1/5/90

John A. Lehman
Principal Investigator

Date: 1/5/90.

A. Husain
Section Head

Date: 1/16/90

D. Lamb
Department Manager

FINAL REPORT

1. **ARO PROPOSAL NUMBER:** 23004-PH-A

2. **PERIOD COVERED BY REPORT:** 1 OCTOBER 1985 - 30 SEPTEMBER 1989

3. **TITLE OF PROPOSAL:** Nonlinear Optical Effects in GaAs/AlGaAs Superlattices Program

4. **CONTRACT OF GRANT NUMBER:** DAAG29-85-C-0028

5. **NAME OF INSTITUTION:** Honeywell Inc.

6. **AUTHOR OF REPORT:** John A. Lehman

7. **LIST OF MANUSCRIPTS SUBMITTED OR PUBLISHED UNDER ARO SPONSORSHIP DURING THIS REPORTING PERIOD, INCLUDING JOURNAL REFERENCES:**

> "Nonlinear Optical Properties of nipi Superlattices", P.P. Ruden, J.A. Lehman, to be presented at SPIE OE-LASE, Los Angles, CA, January 15-19, 1990.
>
> "Optical Modulation of Light Transmission in GaAs Doping Superlattices", P.P. Ruden, J.A. Lehman, N. Khan, M.K. Hibbs-Brenner and E. Kalweit, Journal of Applied Physics 65(8), 15 April 89, 3293.
>
> "Measurement of Intensity-Dependent Carrier Lifetime in Doping Superlattices", A. Chavez-Pirson, S.H. Park, M. Pereira, N. Peyghambarian, J.A. Lehman, P.P. Ruden, and M.K. Hibbs-Brenner, presented at CLEO '89, Baltimore, MD, April 23-28, 1989.
>
> "Determination of the Third Order Nonlinearity as a Function of Quantum Well width in GaAs/AlGaAs Multiple Quantum Wells", M.W. Derstine, D.E. Grider, J.A. Lehman, P.P. Ruden, and Nasser Peyghambarian, SPIE vol 881, Optical Computing and Nonlinear Materials 1988.

John A. Lehman
Honeywell Inc.
Systems and Research Center

Accession For	
NTIS GRA&I	☑
DTIC TAB	☐
Unannounced	☐
Justification	

By_____

Distribution/

Availability Codes

Dist	Avail and/or Special

A-1

TABLE OF CONTENTS

i

1.0 Executive Summary

This report highlights the motivation, results, conclusions and some recommendations of the Nonlinear Optical Effects in GaAs/AlGaAs Superlattices program which was funded by DARPA and monitored by the Army Research Office. Work on this program was conducted at Honeywell's Systems and Research Center in Bloomington, Minnesota over the period from October 1, 1985 through September 30, 1989.

The main purpose of this program was to thoroughly study the nature of the optical nonlinearities demonstrated in GaAs superlattices and show potential for device applications. The nonlinear properties in three main types of superlattices were investigated; GaAs/AlGaAs compositional superlattices, GaAs doping superlattices and GaAs/AlGaAs Hetero-nipi superlattices (Figure 1.0.1). Compositional superlattices were studied because theoretical work done in the area of nonlinear optical effects in multiple quantum wells (compositional superlattices) in GaAs/AlGaAs had evidence to show that due to the special properties of a superlattice, a 100X enhancement in the nonlinearity should be expected over that of bulk GaAs[1]. In particular the dependence of the nonlinearity on the well thickness was studied both experimentally and theoretically. GaAs doping superlattices were investigated because it was believed that large nonlinearities could be induced at very low powers due to the tuneable carrier lifetime. The dependence of the nonlinearity on the power was studied. GaAs/AlGaAs Hetero-nipis were studied as an extention of GaAs doping superlattices.

The nonlinear effects in the three types of superlattices were explored by 1) growing high quality material by MOCVD and MBE, 2) characterizing the nonlinear optical properties using various experimental techniques, and 3) developing theoretical models which predict the superlattice optical behavior. Summarized below are the key results achieved during the investigation of the nonlinear optical properties in GaAs superlattices.

- A systematic study of the dependence of the optical nonlinearities on well thickness for GaAs/AlGaAs compositional superlattices at room temperature shows a ratio of nonlinear refractive index to carrier concentration increases by a factor of 2.5 to 3 as well size decreases from bulk to 47 Å. This is far less than was originally predicted by Chang, nevertheless the nonlinearities are large compared with those of other semiconductors at room temperature.

- State-of-the-Art optical nonlinearities were measured in both the MOCVD and MBE GaAs/AlGaAs compositional superlattices grown at Honeywell. The nonlinear parameters of $\Delta\alpha \approx 1000$ cm^{-1} and $\Delta n \approx 0.15$ were achieved with peak pulsed intensities of $\sim 10^6$ W/cm^2. These parameters were confirmed in a separate experiment performed by Prof. Nasser Peyghambarian at the University of Arizona as part of a subcontract.

- Theoretical models which accurately predict the optical properties and

---

[1]. Y. C. Chang, "Nonlinear Optical Properties of Semiconductor Superlattices", J. Appl. Phys. (58)499, 1985.

1

dynamic behavior in GaAs/AlGaAs compositional and doping superlattices were developed and applied to the design of materials and device structures.

- Very large nonlinear optical parameters ($\sim 1000 \text{ cm}^{-1})^2$ were demonstrated using very low power excitation (0.5 W/cm^2) in GaAs doping superlattices and GaAs/AlGaAs Hetero-nipis. These nonlinearities are as large as any reported in the literature for GaAs doping superlattices and they provide a competitive advantage over composition superlattices as nonlinear material for device applications because the nonlinearities are available at much lower power.

- A light modulator was constructed and successfully demonstrated. The structure consists of a 1 μm thick GaAs doping superlattice sandwiched by GaAs/AlAs superlattice mirrors. This unoptimized structure was grown by MOCVD and provide transmission modulation of 40% which is 4X larger than the modulation observed in a similar doping superlattice without the mirrors. Simple models predict that a 15 to 27dB extinction ratio could be expected in optimized structures showing the considerable device potential for optical signal processing and laser hardening applications.

- An applications study was performed which summarizes the most significant applications of spatial light modulators and outlines the performance required of the modulators in each application.

Because the large nonlinearities in compositional superlattices are a result of exciton saturation, they occur near the band edge where absorbtion is so large that long interaction length devices necessary to increase the effective nonlinearity are not possible without substantial reduction of the transmitted light energy. The nonlinearity features are also very sharp (narrow band) and would be strongly susceptible to changes in temperature. In addition higher powers are required to achieve the large nonlinearities which makes these structures unsuitable for use in high density arrays.

We feel that the more promising candidate material systems for continued research and nonlinear optical device development are the GaAs doping superlattice and GaAs/AlGaAs Heteronipis. Because the of the tuneable nature of the optical and electrical properties of the structure, very low power nonlinearities are possible. Preliminary results from the doping spatial light modulator establish that this device is a viable candidate for use in optical signal processing systems.
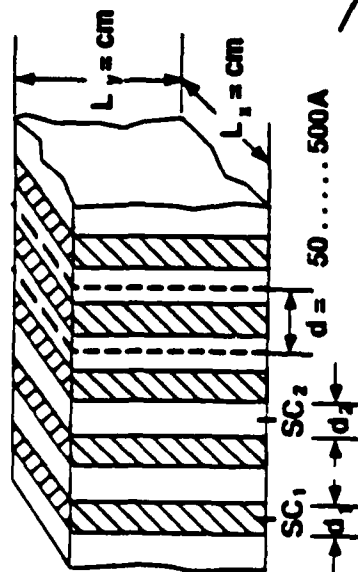
In summary, we feel strongly that the results of this have program have established that, in general, doping superlattices are very promising structures for applications in optical signal processing and warrants further research. More specifically, with its predicted large, low power extinction ratio, we think the GaAs doping superlattice spatial light modulator is an ideal candidate device for use in an optical signal processing system and warrants further research.

---

2. This power is an upper limit. Large changes in nonlinearity may in fact occur at much lower powers (10-100X less) which is describe later in this report.
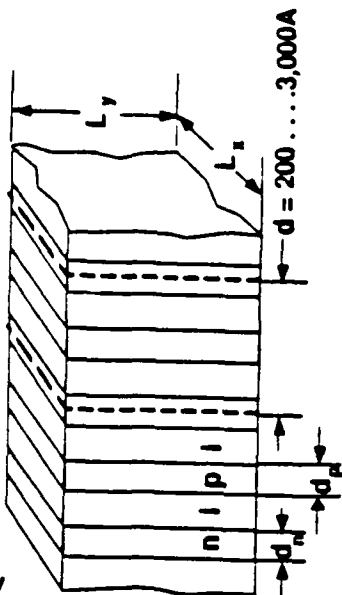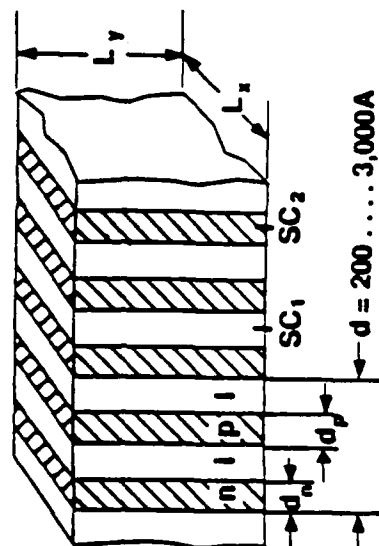
Superlattices

Doping (n-i-p-i)

$d = 200 \ldots 3{,}000A$

L_y
L_x

d_p
d_n
n | p |

- Low power optical nonlinearities
- Wide wavelength band

Compositional

$L_y \approx cm$
$L_x \approx cm$

$d = 50 \ldots 500A$

SC_1
SC_2
d_2
p |

- Large optical nonlinearities
- Narrow wavelength band
- High absorption

Hetero-nipi

L_y
L_x

$d = 200 \ldots 3{,}000A$

SC_1 SC_2

d_p
d_n
n | p |

- Large optical nonlinearities
- Low power
- Low absorption at operating wavelengths

Figure 1.0.1

1.1 Introduction

Work on the Nonlinear Optical Effects in GaAs/AlGaAs Superlattices program, contract #DAAG-29-85-C-0028, funded by DARPA and monitored by ARO, was conducted at Honeywell's Sensors and Signal Processing Laboratory over the period from October 1, 1985 to September 30, 1989. This period of performance includes two no-cost extensions. Significant contributors to this program have been:

> Mr. John A. Lehman
> Dr. P. Paul Ruden
> Dr. Matthew Derstine
> Dr. Mary Hibbs-Brenner
> Ms. Nisa Khan
> Dr. Julian Bristow
> Dr. David Grider
> Dr. Paul Kruse
> Dr. David Arch
> Dr. Jon Abrockwah

In addition to the above Honeywell researchers, Professor Nasser Peyghambarian from the University of Arizona acted as consultant on this program by assisting in the understanding of the mechanisms responsible for the superlattice nonlinearities as well as providing independent nonlinear optical measurements to Honeywell's results. This report is divided into three main sections. Section 2.1 deals with the nonlinearities in GaAs/AlGaAs compositional superlattices and the comparison of these nonlinearities with various well thicknesses. Section 2.2 handles the research done on the optical nonlinearities in GaAs/AlGaAs doping superlattices. The main body of this report concludes in section 2.3 by suggesting a possible spatial light modulator (SLM) device configuration which makes use of the large changes in absorption below the band edge in a GaAs doping superlattice. Preliminary modeling calculations are provided to show performance. An attachment is provided which summarizes significant applications of spatial light modulators and outlines the performance required of the modulators in each application.

The level of effort of research between the Compositional and Doping superlattices was roughly equal; the first two years concentrating on the compositional superlattices and the final two years concentrating on doping superlattices.

2.0 Nonlinear Optical Effects in GaAs Superlattices

During this program, nonlinear optical effects were investigated in both GaAs/AlGaAs compositional and Doping Superlattices. Theoretical work leading to models which predicted the magnitude and spectral character of the nonlinearities as well as experimental work to measure the nonlinearities were conducted on both types of superlattices.

2.1 Comparison of Optical Nonlinearities of Bulk GaAs and GaAs/AlGaAs Superlattices with Various Well Thicknesses.

GaAs/AlGaAs superlattices belongs to a class of semiconductor structures where the band gap and therefore certain novel optical and electrical properties can be "engineered" through judicious design of the GaAs and AlGaAs layer thicknesses and AlGaAs composition. Figure 2.1.1 shows schematic representations of the different types of superlattices. Quasi-two-dimensional behavior is produced by sandwitching the low-gap GaAs between the higher-gap AlGaAs layers. If the AlGaAs layers are thick enough and have sufficiently high aluminum composition, the excited carriers will be forced to travel in the x-y plane of the GaAs layer. Motion in the direction perpendicular to the layers is quantized. The quasi-two-dimensional effects are observed when the GaAs thickness is less than approximately that of twice the exciton Bohr radius.

$$2a_{3D} = \epsilon h^2/a^2\mu^* \sim 300\text{Å} \tag{1}$$

This confinement of the motion to a plane is sufficient to largely enhance excitonic effects. Sharp excitonic resonances have been observed in GaAs/AlGaAs superlattices at room temperature while they are not easily observed in bulk GaAs. This is so because the two-dimensional confinement in the superlattice increases the excitonic binding energy such that it is not easily thermally ionized whereas the bulk GaAs excitons have a much lower excitonic binding energy and are thermally ionized almost immediately after they are formed. Because these excitonic resonances are easily saturated the nonlinearities associated with the resonances are very large. The mechanisms responsible for the resonant
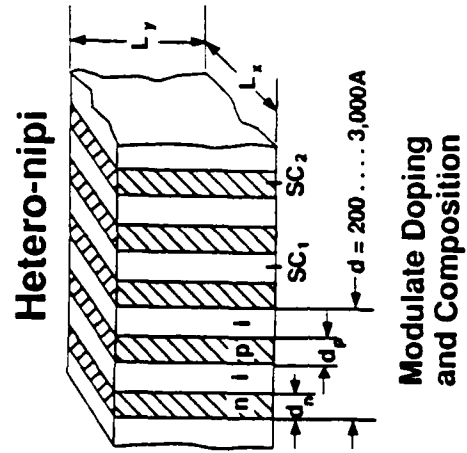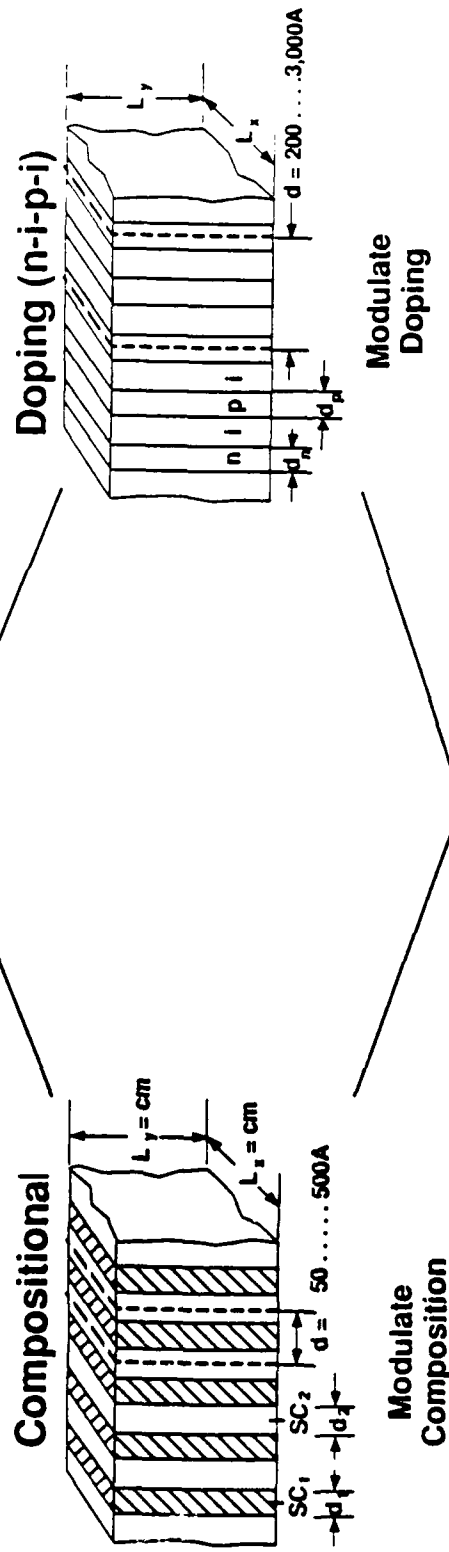
4

Superlattices

Figure 2.1.1   Diagram of GaAs/AlGaAs Compositional Superlattice, GaAs Doping Superlattice, and GaAs/AlGaAs Hetero-Doping Superlattice.

5

nonlinearities in the GaAs/AlGaAs compositional superlattice are screening of the bound and continuum exciton states, band filling and band gap renormalization where the effective nonlinearity is the sum of the components of the different mechanisms and are dependent on the number of photoexcited electron-hole pairs.

The focus of this work done on the compositional superlattice was to investigate the relationship between the GaAs well thickness and the optical nonlinearity. As mentioned in the foreword, it was expected that narrow well superlattices (~50A) would have a much larger (~100x) nonlinearity than bulk material. To understand this relationship eighteen GaAs/AlGaAs samples were grown with different design parameters. Table 1 shows these samples.

Table 1.

sample	GaAs well width	AlGaAs barrier width	periods	growth	comments
465	60 Å	60 Å	100	MBE	
466	60	120	60	MBE	
260	80	80	60	MOCVD	
262	80	120	60	MOCVD	
463	100	100	50	MBE	
248	100	100	60	MOCVD	
261	120	120	60	MOCVD	
674	47	52	100	MBE	
675	103	105	50	MBE	
676	149	158	34	MBE	
677	299	296	17	MBE	
678	5000	5000	1	MBE	bulk
680	103	105	100	MBE	interrupt growth tech
328	100	100	75	MBE	
329	100	100	75	MBE	
149	100	100	75	MBE	
464	100	100	60	MBE	

Superlattices were grown with GaAs well thicknesses varying from 47A to 299A.

In addition one bulk GaAs sample was grown. Samples were grown using both MBE and MOCVD techniques. A Physical Electronics PHI 425A MBE system was used to provide the 3" diameter wafers while the MOCVD reactor was an in-house design and provided 1"x2" square samples. An interrupted growth technique was used on sample 680 to determine if quantum well interface abruptness had any effect on the nonlinear optical properties. All layers were grown intrinsically undoped or lightly doped with Si to compensate the material and reduce the number of free carriers.

Theoretical Calculations

Calculations were done which estimated the excitation dependence of the interband optical absorption in a GaAs/AlGaAs multiple quantum well. The exciton binding energies and oscillator strengths were calculated for GaAs/AlGaAs MQW structures using a variational approach. Excitons were treated as quasi-two-dimensional, allowing for non-zero average distance between the electron and hole in the direction perpendicular to the layers but neglecting the Coulomb correlation in this direction. Screening by free electrons and holes was included within a two-dimensional Debye approximation. Together with the previously determined subband structures and the carrier density dependent band gap renormalization, the interband absorption coefficient was evaluated. We treated the Coulomb enhancement of the continuum absorption in a manner analogous to the screened exciton. Results for the ground state and for a non-equilibrium carrier concentration of 10^{11} cm^{-2} are shown in Figure 2.1.2. The superlattice parameters for this calculation were 100A for the thicknesses of both types of layers and an alloy composition of 0.45. Gaussian lineshapes were assumed with a width of 7 meV. The difference between the two absorption spectra is shown in Figure 2.1.3. An experimental absorption spectra and change in absorption spectra are compared with predictions in Figure 2.1.4. Although the magnitude of the calculated spectra are much larger than the measured spectra, the difference can be explained by the large oscillator strengths and the large non-equilibrium concentrations which were used in the calculations. Closer agreement in magnitude could be achieved by adjusting the variable parameters in the model such that the magnitudes of the prediction and the experiments would be more equal, however for purposes here it

7

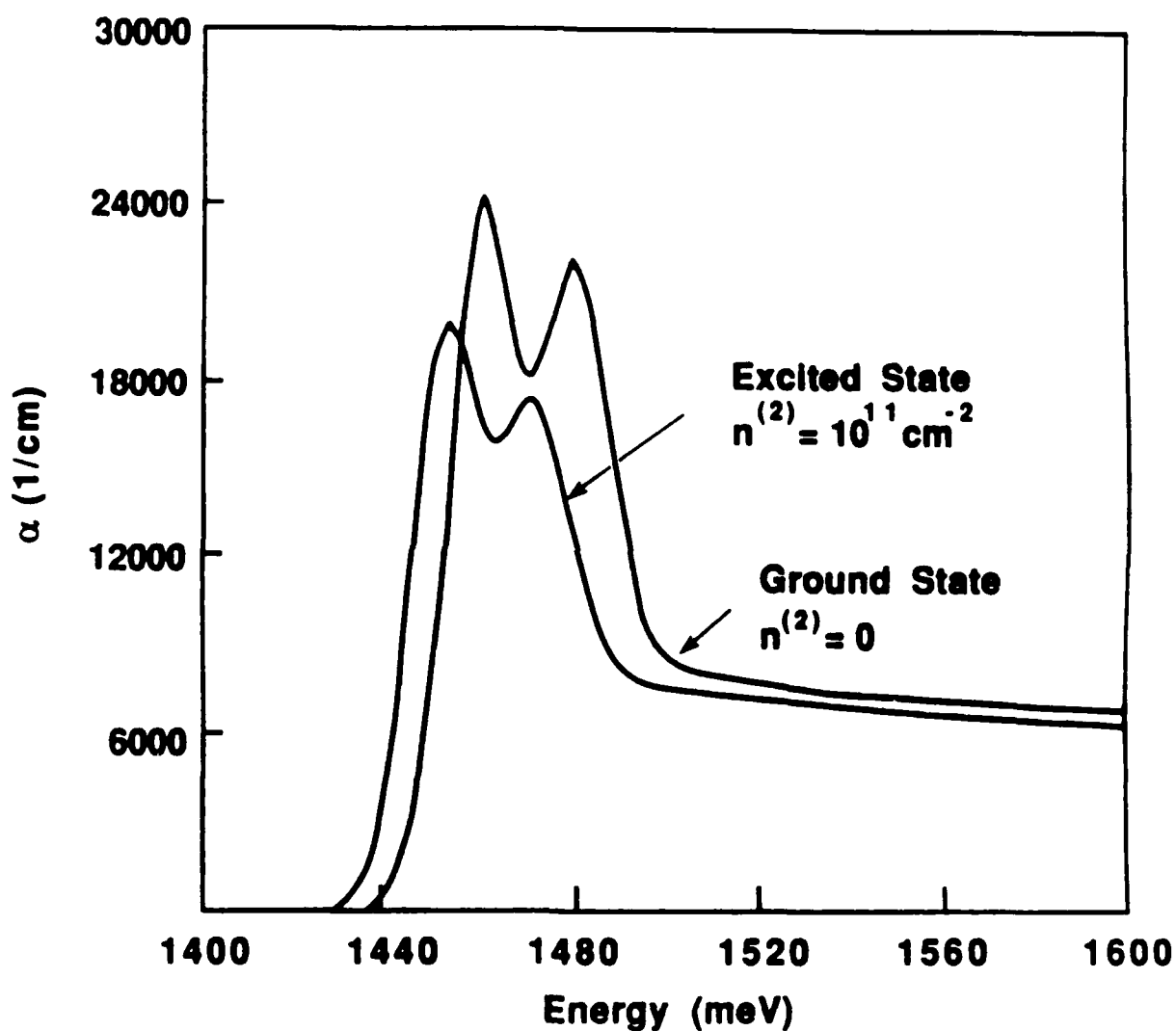# Theoretical Calculation of Absorptive Nonlinerarity

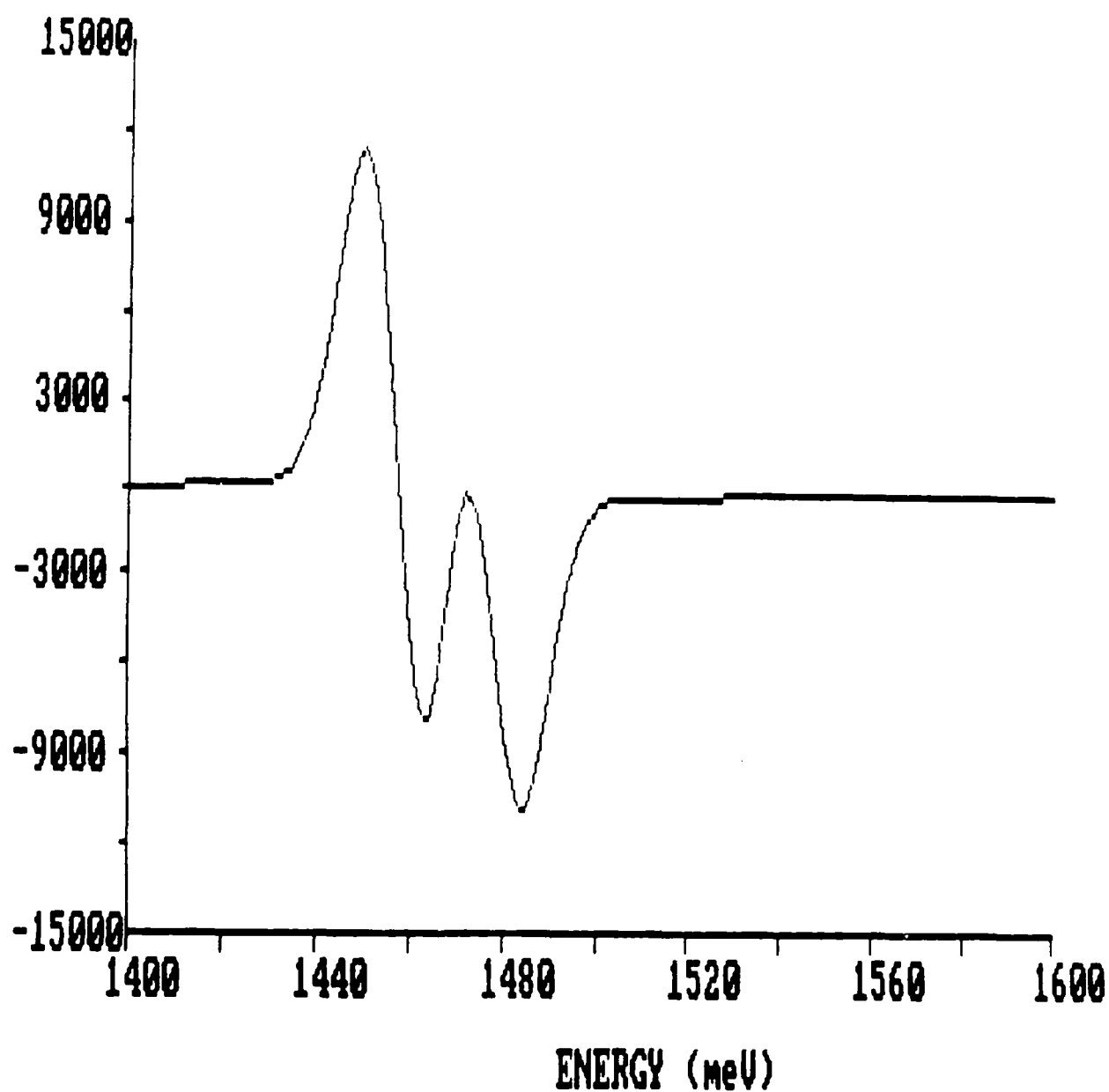Figure 2.1.2   Theoretical Calculation of Absorptive Nonlinearity

Figure 2.1.3   Theoretical Calculation of delta absorption for a nonequilibrium carrier concentration of 10^{11} cm^{-2}.

Comparison of Theoretical and Experimental Results for Compositional SL Nonlinearity

Prediction

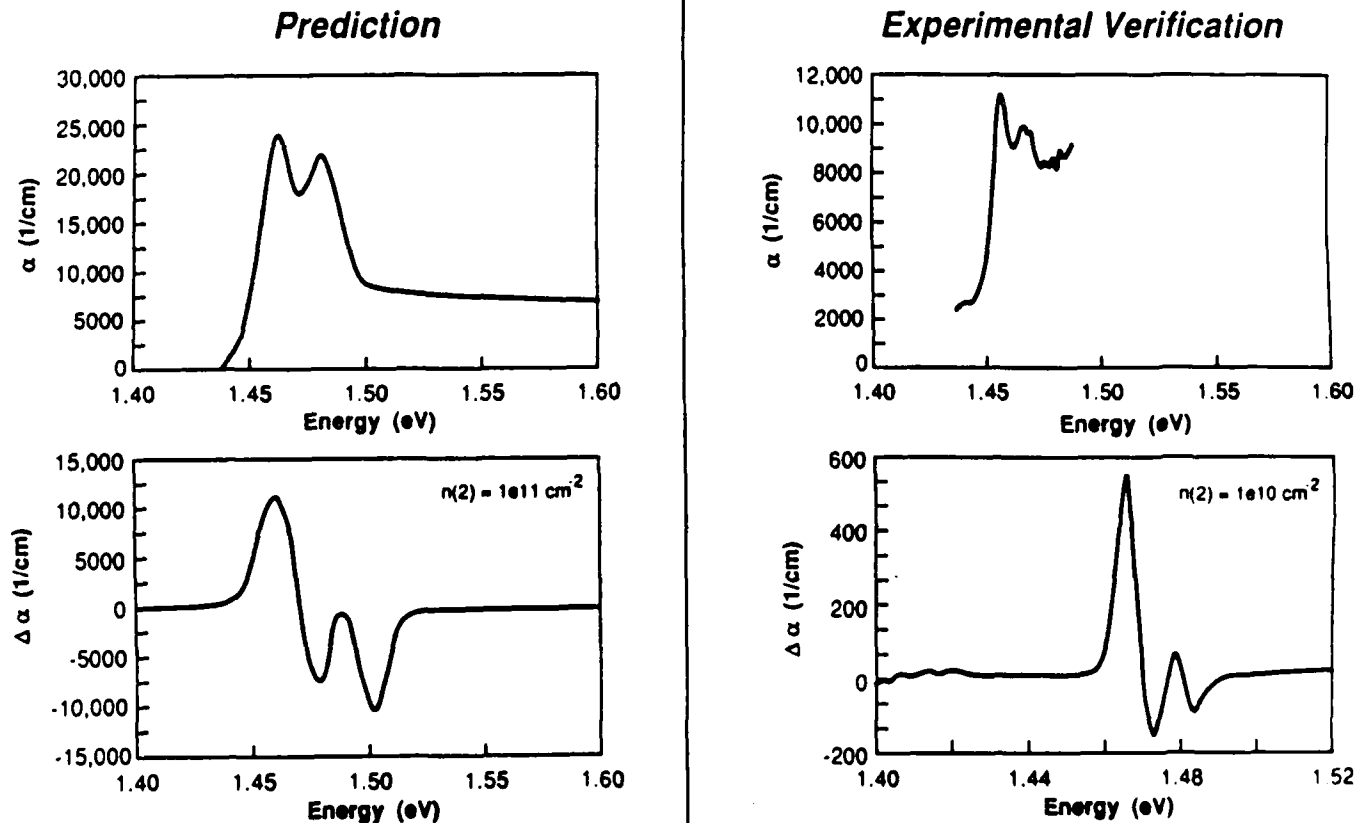### *Experimental Verification*

Figure 2.1.4   Comparison of theoretical and experimental results for compositional superlattice.

10

was not thought to gain us any further insight into the problem.

Nonlinear Optical Measurements

The principal effort in this program was placed in the nonlinear characterization of the samples. Two techniques were used to accomplish this task: Degenerate four-wave mixing and nonlinear transmission/absorption experiments. The techniques were used together to arrive at the nonlinear optical parameters. In addition, by using picosecond light pulses, material dynamics such as carrier lifetime and ambipolar diffusion could be investigated. Honeywell conducted the four-wave mixing experiments and some of the nonlinear transmission experiments while the University of Arizona performed nonlinear absorption measurements.

The nonlinear characterization at Honeywell was conducted using a Spectra-Physics 171 mode-locked Ar^+ laser pumping a cavity-dumped dye laser as the light source. The output of this system provided 5-10 picosecond pulses at 4 MHz, was tunable from 790nm to 910nm and was computer controlled. The short pulse widths were useful when doing time resolved studies of the grating lifetime.

A standard pump/probe configuration was used to do the four-wave mixing experiments. In this configuration, a strong pump beam and a weak test beam are focused onto the same spot on the sample and interfere with each other creating periodic regions of high intensity light. These high intensity regions photo-excite carriers which in turn alter the refractive and absorptive characteristics of the sample, thereby producing an amplitude and phase grating. By measuring the diffraction efficiency of this grating, the change in the index and absorption can be obtained. By measuring the change in the transmission through the sample of the test beam due to the pump, $\Delta\alpha$ can be obtained and by measuring the linear transmission and reflection, the linear absorption can be calculated. Because of the tunability aspects of the dye laser, all of the measurements were taken as a function of wavelength. A diagram of the experimental set-up is shown in Figure 2.1.5.
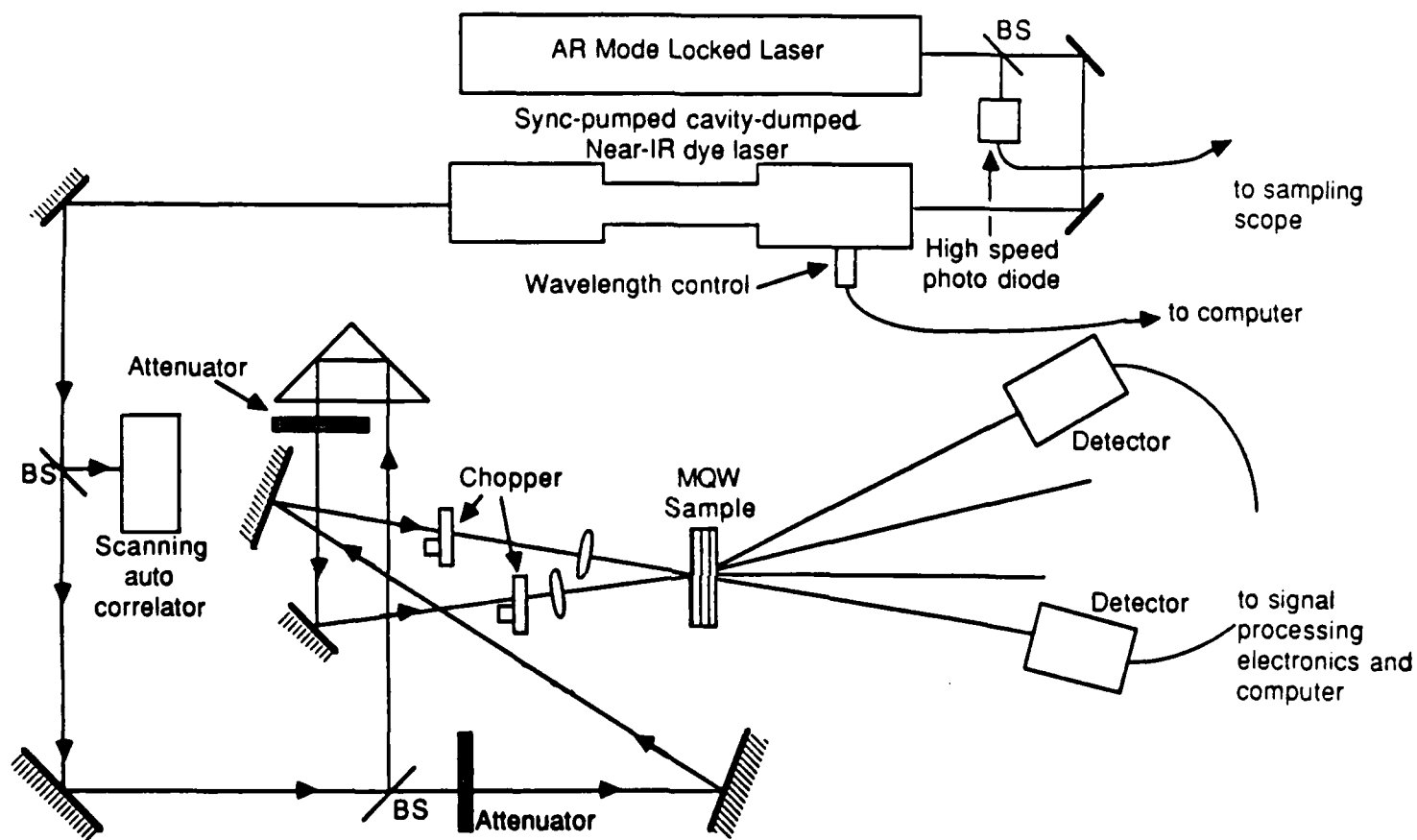
11

NLO Experimental Setup

Figure 2.1.5   Diagram of degenerate four-wave mixing experimental setup.

Due to the low power of the signal relative to the transmitted pump beam, it was necessary to do some signal processing on the diffracted beam to pull the signal out of the background scatter. To do this we made use of a dual lock-in scheme which filters out both the pump and test beam scatter. The lock-ins were referenced to two optical choppers which were placed in the pump and test beam paths. The two choppers had angular frequencies of 1.1kHz and 80 Hz respectively.

The data acquisition of the four-wave mixing and nonlinear absorption experiments was computer controlled and the data was stored on floppy disks. The program varied the dye laser wavelength, measured the four-wave mixing and nonlinear absorption signals, measured the linear transmission and reflection signals and monitored the pump power. Because the computer could do the routine and monotonous tasks of recording data, more points could be taken so that better resolution was possible.

DFWM experiments were performed on all the samples in Table 1. Typical experimental results are shown in Figures 2.1.6 - 2.1.7. Figure 2.1.6a shows a DFWM signal spectrum for a fixed test and pump power. Note the two separate peaks in the spectrum. The larger peak arises from the heavy-hole exciton nonlinearity while the smaller peak is due to the light-hole exciton nonlinearity. Figure 2.1.6b shows a delta transmission spectrum. The two positive changes in transmission result from the saturation of the heavy and light hole exciton resonances which can be seen in the absorption spectrum in Figure 2.1.6c. The negative peak is due from the red shift of the bandedge which accompanies bandgap renormalization. Figure 2.1.7a displays the large change in index per photoexcited electron-hole pair ($n_{eh} = \Delta n/N$). For this plot $\Delta n \approx 0.018$ and $N \approx 3 \times 10^{16}$ cm^{-3}. Figure 2.1.7b shows the change in absorption per photoexcited electron-hole pair. Here, $\sigma_{eh} = \Delta \alpha/N$ and $\Delta \alpha \approx 1800$ cm^{-1} at the heavy hole exciton peak.

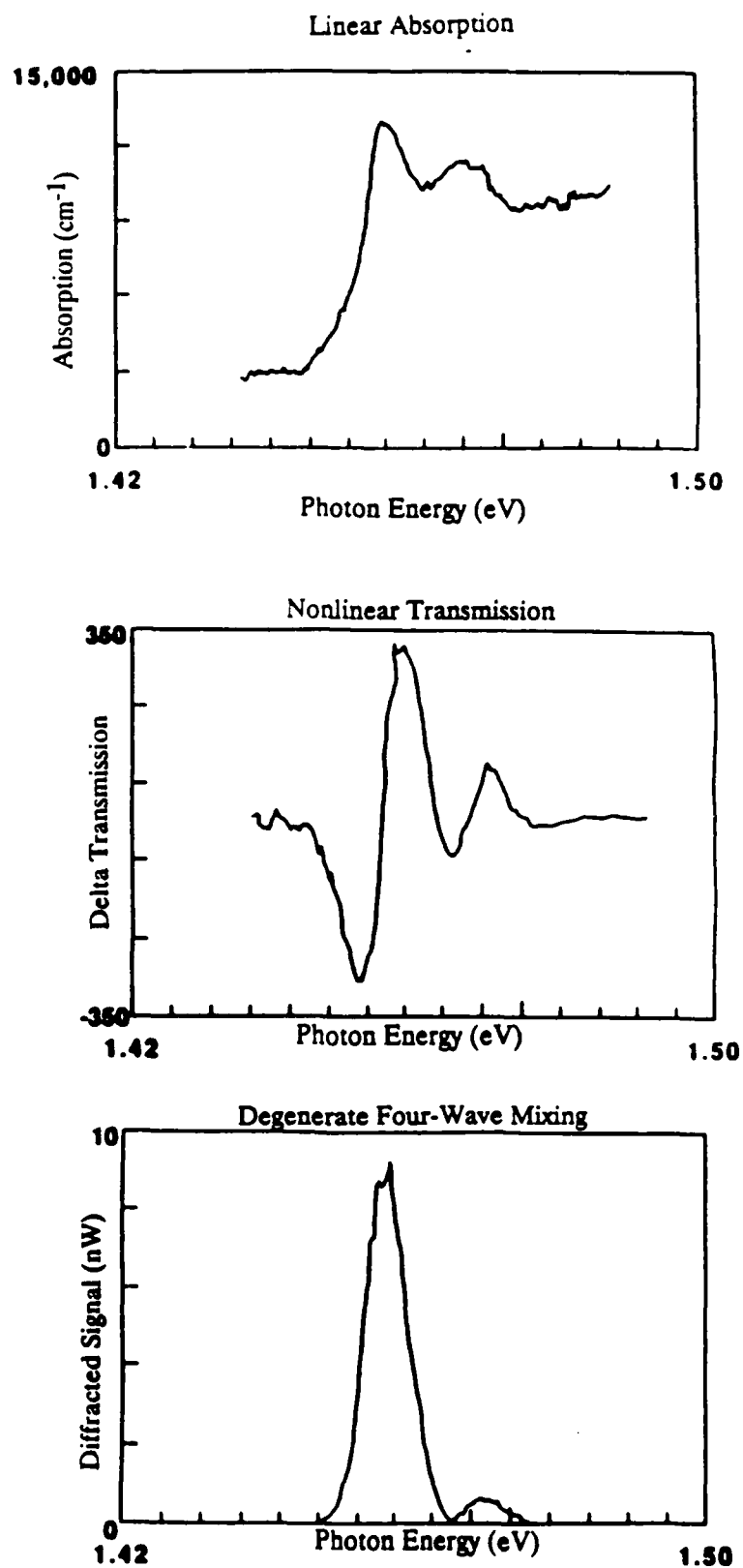## Linear Absorption

Nonlinear Transmission

Degenerate Four-Wave Mixing

Figure 2.1.6

14

Absorptive Nonlinearity $\qquad \sigma_{eh} = \Delta\alpha/N$

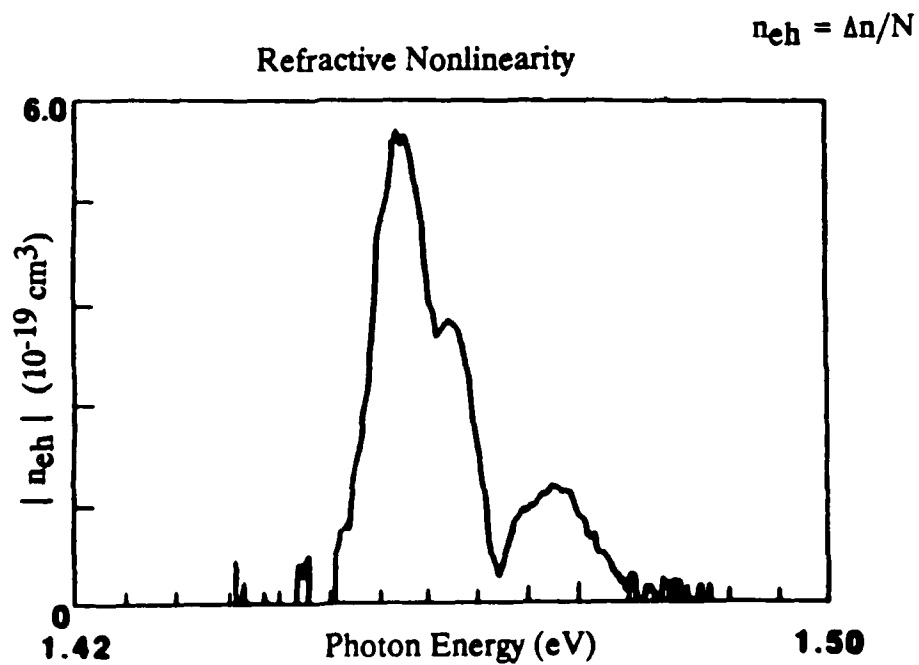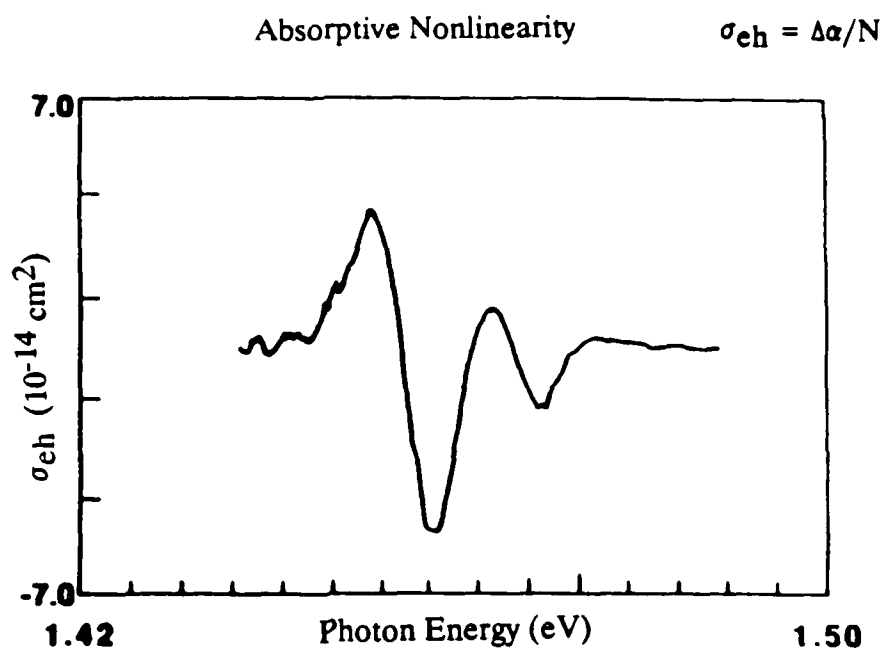Refractive Nonlinearity $\qquad n_{eh} = \Delta n/N$

Figure 2.1.7

15

Carrier Diffusion Measurements

The diffraction of light from the grating formed by the interference of the pump and test beams provide an excellent technique for determining the ambipolar carrier diffusion within the GaAs/AlGaAs superlattice. Once the refractive and absorptive gratings are formed, the photoexcited carriers which are heavily concentrated in the "bright" part of the grating will diffuse to the region where the concentrations are much less. When this happens the modulation of the grating decreases. By probing the grating with a low power beam and measuring the diffraction efficiency at different times after the grating is first created, one can gain an understanding of the carrier diffusion properties.

In our experimental configuration the grating lifetime associated with the ambipolar diffusion is:

$$\tau_D = [\lambda/4\pi \sin(\theta/2)]^2 D^{-1} \qquad (2)$$

where θ is the angle between the beams creating the grating. Our setup, shown in figure 2.1.8, uses a third beam to probe the grating created by the other two beams. The third beam has a variable path length used to probe at different times after the creation of the grating and is cross-polarized so that no interference between the pump beams and the probe take place. Figure 2.1.9 shows a typical decay of the diffraction efficiency. From the plot of diffraction efficiency vs. time delay a time constant is extracted and using the equation 2 the diffusion coefficient is obtained. Our results show that the MBE samples have a larger diffusion coefficient than the MOCVD samples and the newest MBE samples (where the samples are of higher quality) have the largest diffusion coefficients.

Because a sample with a large diffusion coefficient has a shorter grating lifetime than a sample with a smaller diffusion coefficient it might be expected that for certain pump/test angles the larger diffusion coefficient sample would have a smaller diffraction efficiency. The larger the pump/test beam angle the more closely spaced are the grating fringes within the sample. A grating with narrowly spaced fringes will decay faster due to the diffusion of the carriers which washes
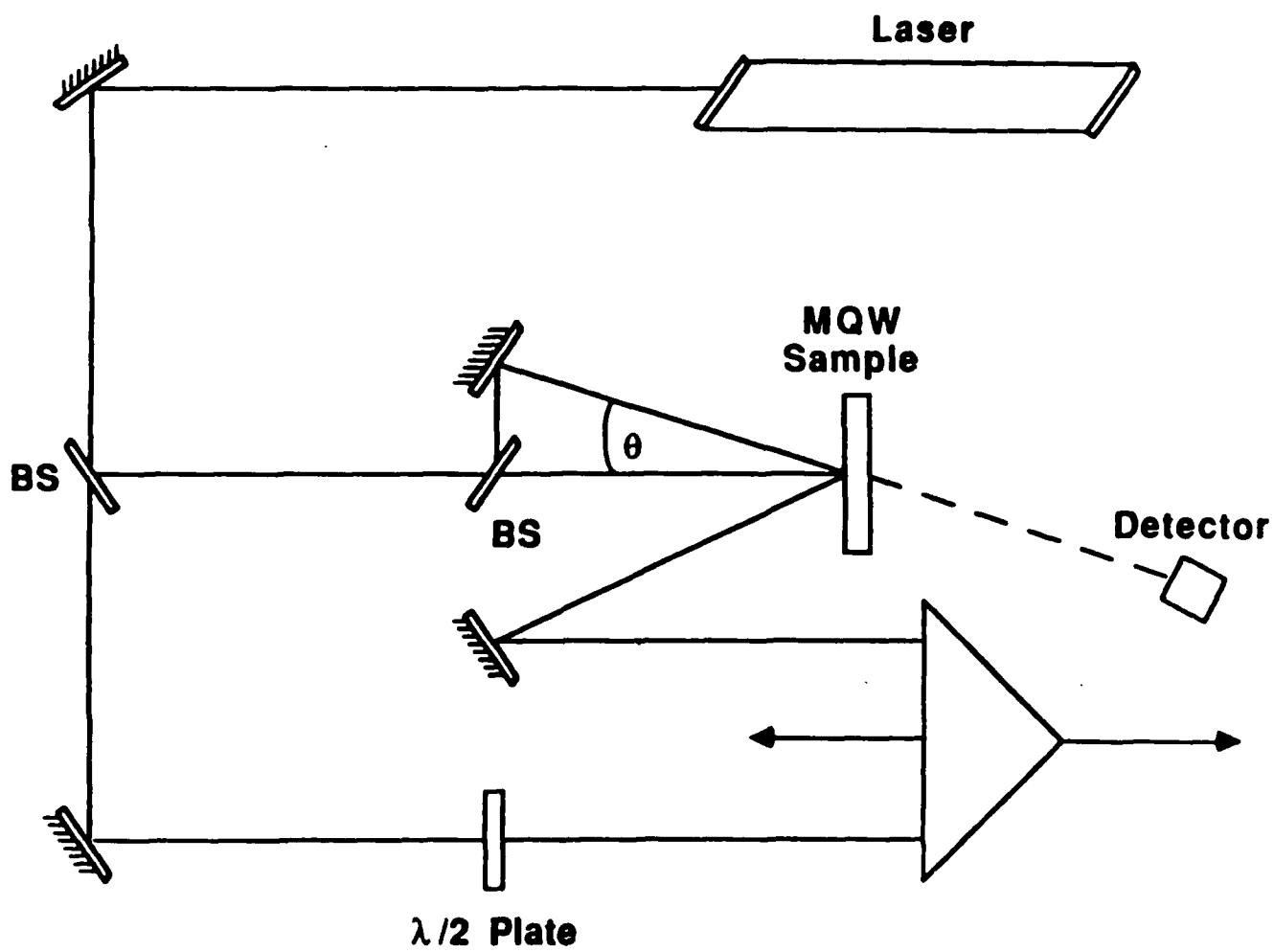
16

Figure 2.1.8   Experimental configuration for grating lifetime measurement.
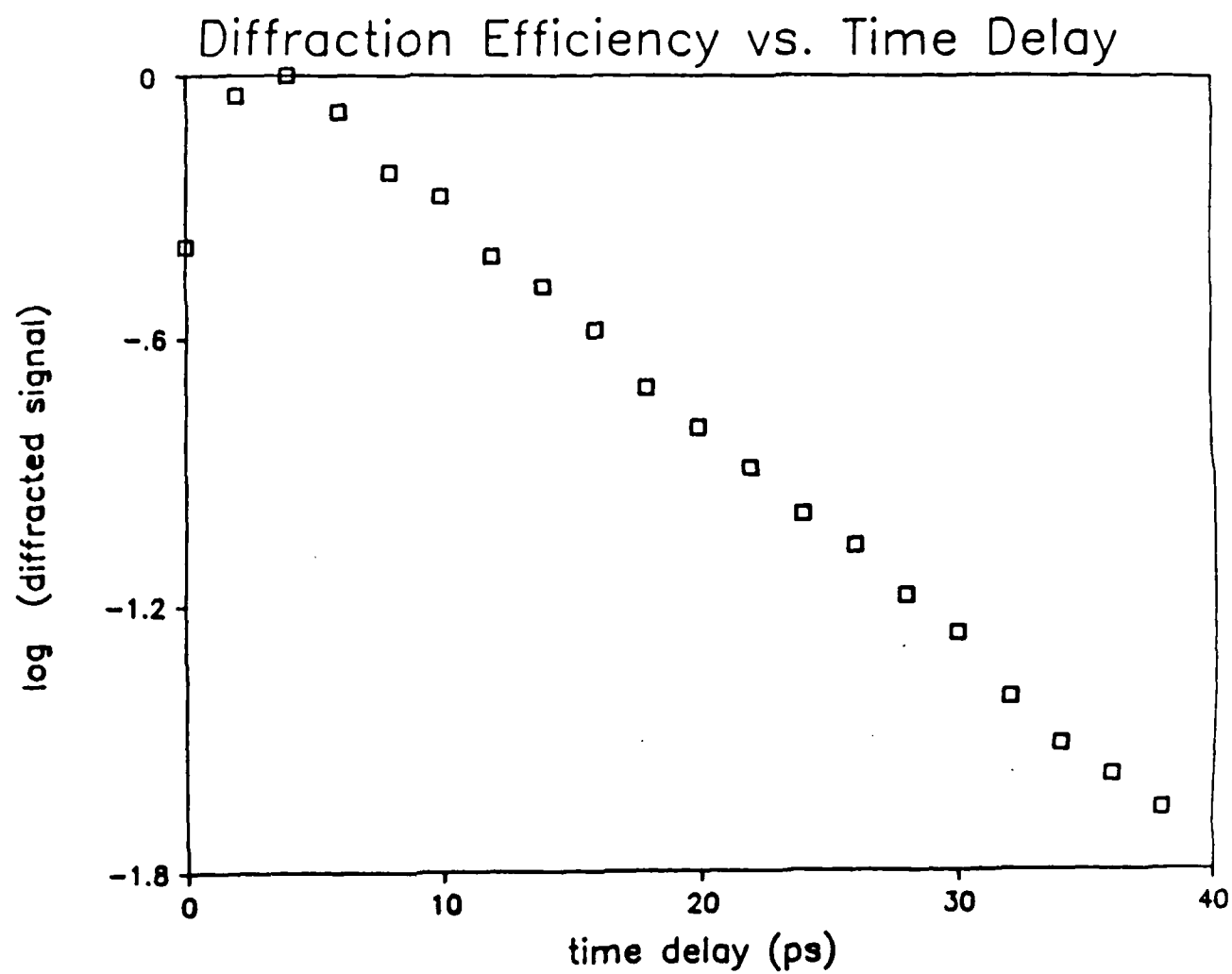
Figure 2.1.9   Diffraction efficiency vs. probe time delay.

18

out the diffraction grating.

Although it seems reasonable that this effect should happen, to show it experimentally was difficult. A sample might have a large or a small diffraction efficiency for reasons other than the extent of the grating decay which is due to diffusion. Nevertheless we took two samples which had the same design parameters but had different diffusion coefficients and measured their diffraction efficiencies using degenerate four-wave mixing. (One sample was grown at the beginning of the program while the other was grown about two years later. Because of the advances made in our MBE growth technique the newer sample was considered to of much higher material quality.) The newer of the two samples had a diffusion coefficient of 60 cm^2/s while the older had a diffusion coefficient of 14 cm^2/s. Calculations showed that for a 10 ps laser pulse the sample with the larger diffusion coefficient would experience a decay in the diffraction efficiency of 85% while the other sample would experience a signal decay of 96%. Therefore the sample with the larger diffusion coefficient should have 89% of the signal that the other sample has. In practice the sample with the smaller diffusion coefficient had more than 2x the diffraction efficiency. This effect would be somewhat enhanced by increasing the angle between the probe and the pump and reducing the grating spacing. Likewise the effect could diminished by reducing the pump/probe angle.

Nonlinear Optical Effects using a Laser Diode

For the previous nonlinear transmission experiments, the pump and test beams were the same wavelength. Therefore as the pump/test wavelength was varied, the number of photoexcited carriers varied depending on the material absorption at that wavelength. Above the band edge where the absorption is large, more carriers were excited while below the band edge where the band edge is smaller, far fewer carriers were excited. As a result, for a given pump power the $\Delta\alpha$ spectra is distorted. A more accurate spectra was obtained by replacing the dye laser pump beam with a pump of a fixed wavelength. For this experiment we used a Hitachi AlGaAs laser diode which had an output at 827.8nm at room temperature and at a drive current of 90mA. The output was collected and focused coincident with the test beam onto the sample. The transmission was detected using a Si

19

photodiode and the signal was acquired and stored by a PC. A lock-in amplifier was used after the detector to increase the signal-to-noise ratio. A typical scan is shown in figure 2.1.10. Compared against previously measured Δα spectra, the below bandgap peak is much larger relative to the above bandgap peak.

Nonlinearity vs. Well Width

A systematic study of the absorptive and refractive optical nonlinearities vs. GaAs (well) thickness was done to see if as theorized, a thin well superlattice would have larger nonlinearities. As mentioned in the Foreword, nonlinearities in the superlattices were expected to be as much as 100X greater than those in bulk. Our results showed that only a factor of three increase in nonlinearity exists in a thin well superlattice (47Å) over that measured in a bulk sample. This data is displayed in figure 2.1.11. The reason for the less than expected difference in nonlinearities between bulk and superlattice can be understood by remembering that the total nonlinearity is sum of the individual component mechanisms. The mechanisms responsible for the third-order optical nonlinearities are Coulomb screening of the excitons, band filling and bandgap renormalization. Although the GaAs/AlGaAs superlattice exhibits sharp exciton resonances at room temperature which are not easily observable in bulk GaAs at room temperature, the efficiency of the Coulomb screening of the resonance in the 3-D system is much greater than the efficiency of screening in the 2-D system. This has a net effect of balancing the nonlinearities in the 2-D and 3-D systems.

University of Arizona Consulting Work

Professor Nasser Peyghambarian consulted on this program by preforming nonlinear optical measurements on our samples. Dr. Peyghambarian used the standard pump and probe method to obtain absorption spectra for various pump intensities. A tunable dye laser operating at 816 nm was used for the pump beam, and the broadband spontaneous luminescence, emitted by a cell containing IR-144 or HITC dye, was used for the probe beam. Both the dye laser and the dye cell were pumped synchronously by the same nitrogen laser, producing 3 nsec full width at

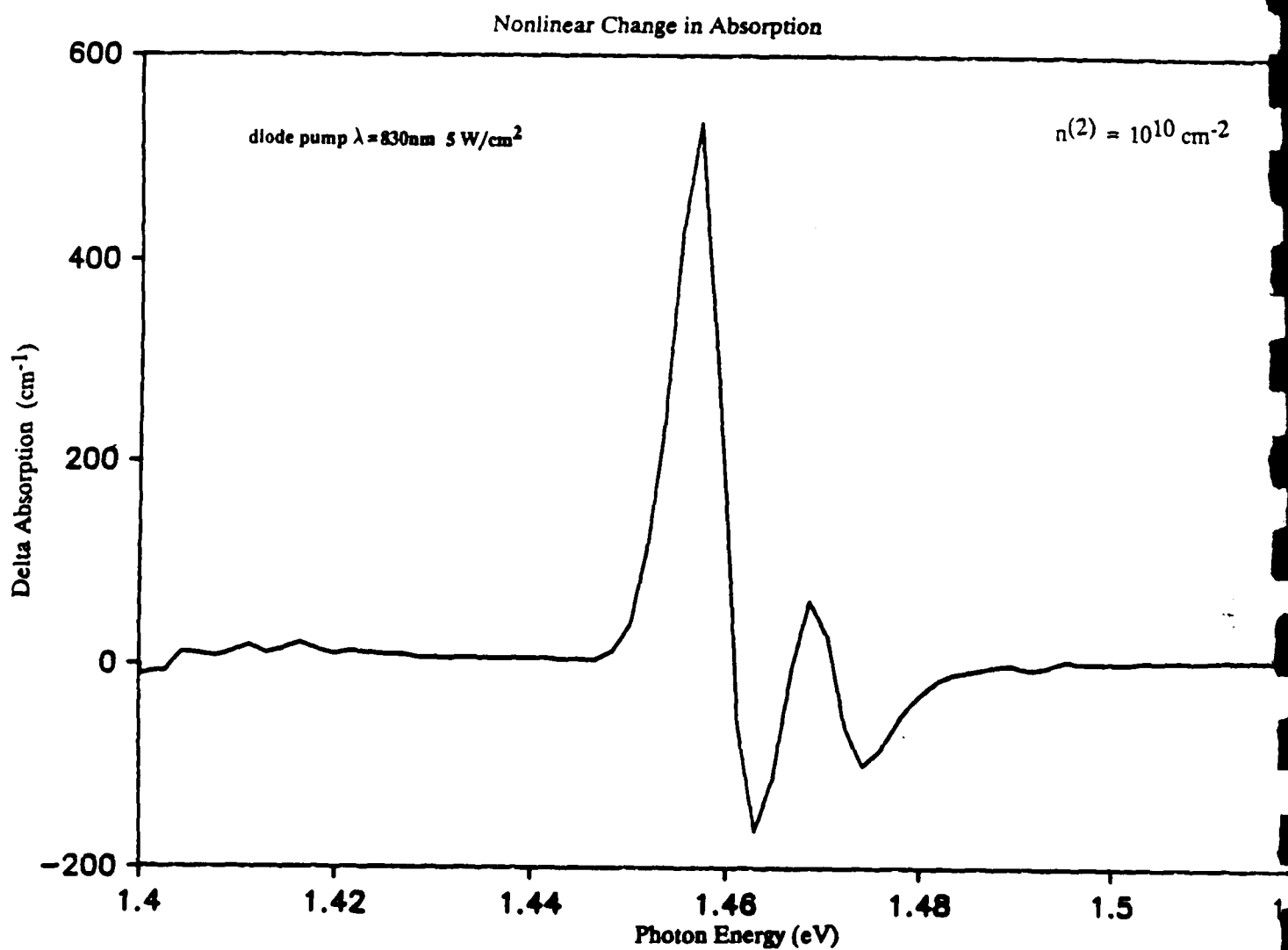Figure 2.1.10   Change in absorption for above bandgap (λ = 830nm) diode pump.

21

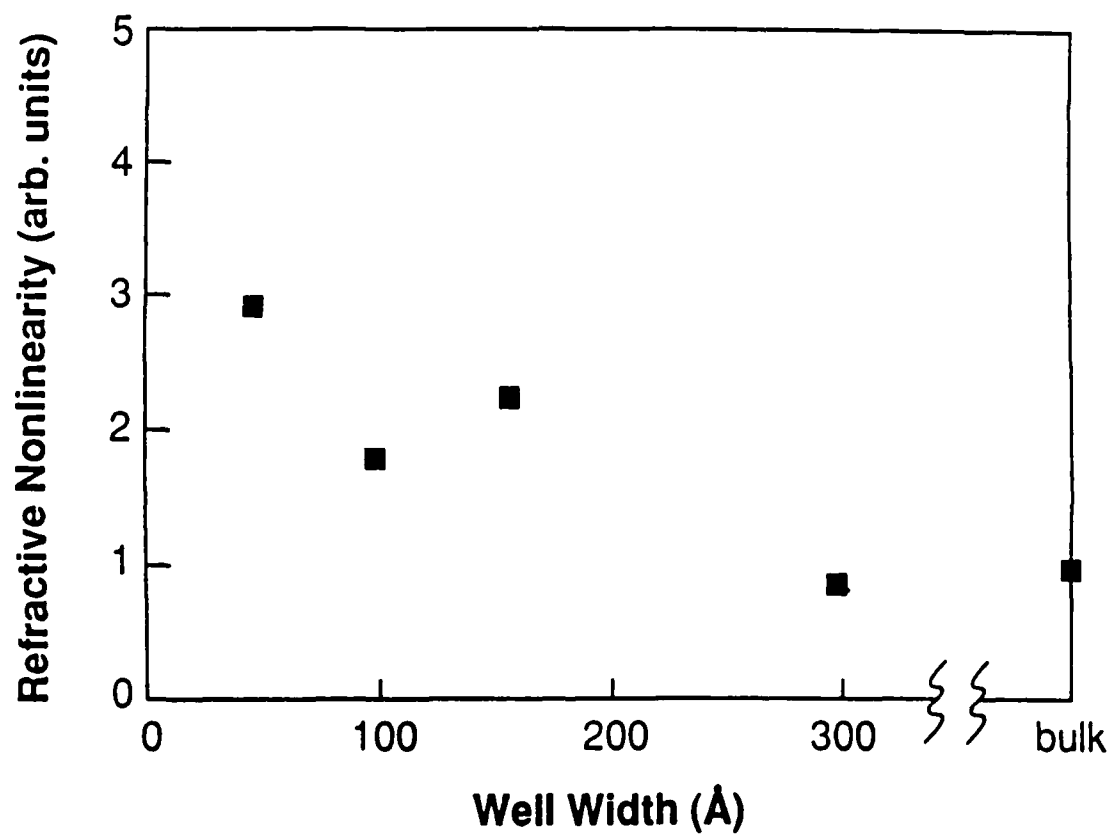# Nonlinearity vs. Well Width for GaAs/AlGaAs Superlattice

Figure 2.1.11   Comparison of refractive nonlinearity vs superlattice well thickness for several samples.

half maximum pump and probe pulses. Various samples, grown by molecular beam epitaxy under identical conditions (in order to reduce variations in sample quality) were studied. The thicknesses of the GaAs well layers in these samples were 47 A, 130 A, 149 A, and 299 A. A sample of bulk GaAs was also studied for comparison with MQW's.

The probe transmission was measured as a function of probe frequency for various pump intensities for each sample. The change in absorption coefficient, $\Delta\alpha$, was then obtained from these spectra. The nonlinear index change, Δn, was calculated from the measured $\Delta\alpha$ using Kramers-Kronig transformation. The results of Δn vs. pump intensity is shown in Figure 2.1.12. As the intensity increases, the bandgap and exciton absorption bleaches, leading to an increase in Δn. Note from Figure 2.1.12 that for a given Δn, a lower pump intensity is required for the 47 A MQW sample than for the bulk sample. These results indicate that the smaller MQWs have larger nonlinear refractive indices. However we will argue below that the comparison of intensity-dependent index changes is somewhat misleading. For resonant excitation, one should always compare carrier-density dependent changes, since the optical material properties depend on the excitation intensity only through the carrier density.

The various samples have a different absorption at the pump frequency so that the same excitation intensity generates a different number of carriers. To obtain a sensible comparison of the material nonlinearities we compute the index change per excited carrier, $\Delta n/N$. Figure 2.1.13 shows the maximum $\Delta n/N$ vs carrier concentration. The carrier concentration is obtained using the simple rate equation:

$$dN/dt = \alpha(\omega_{pump})I/h\omega_{pump} - N/\tau \qquad (3)$$

where τ is the lifetime of the electron-hole pairs, ω_{pump} is the frequency of the pump beam and $\alpha(\omega_{pump})$ is the linear absorption coefficient measured at the pump frequency. Assuming a Gaussian temporal profile for the pump beam, above equation yields
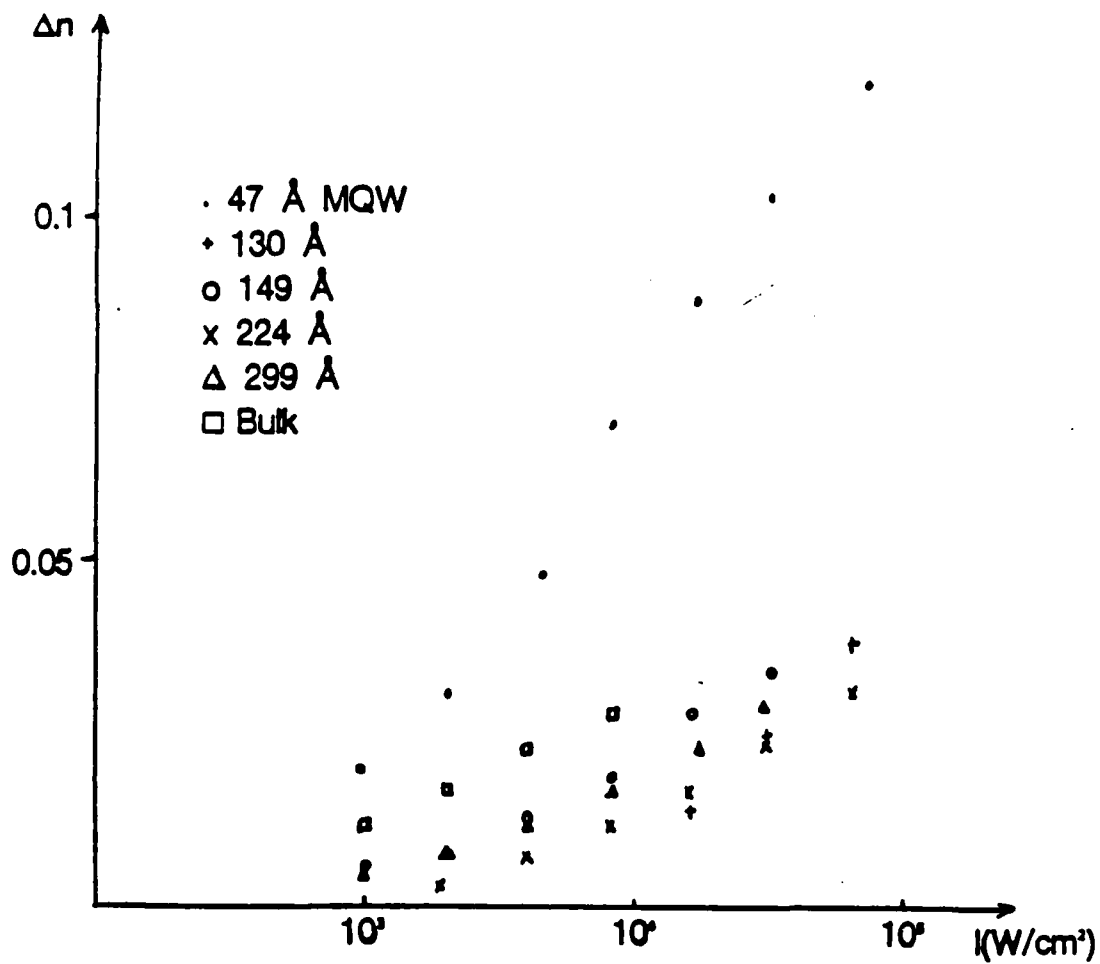
Figure 2.1.12   The measured change in index of refraction as a function of pump intensity for several superlattices and a bulk sample at room temperature.
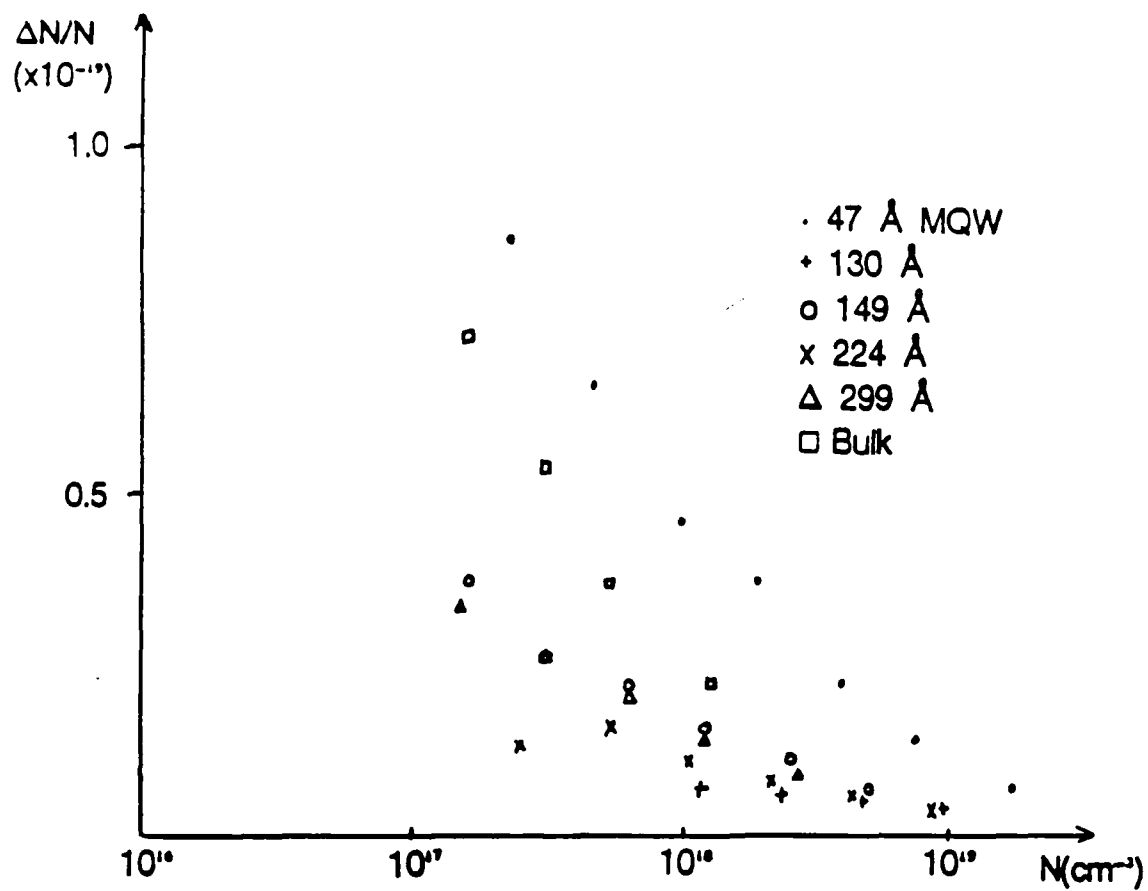
Figure 2.1.13   Measured Δn/N vs. carrier density for several samples at room temperature.

$$N(t) = \frac{e^{-t/\tau} \alpha(\omega_{pump}) I_0}{\hbar \omega_{pump}} \int_{-x}^{t} e^{t'/\tau} \exp -\left[\frac{const.}{(FWHM)} t' \right]^2 dt' . \qquad (4)$$

where I_0 is the peak pump intensity, x is chosen to be twice the FWHM, t is the delay time between the pump and probe, and const = 1.16651. For this experiment, t is 1 nsec, FWHM is 3 nsec, and the carrier lifetime is substantially longer than the 3 nsec pulse width. However recent measurements by A. Chavez-Pirson et al. indicate that the recovery-time of the optical nonlinearities does indeed decrease with decreasing well size. If we include this result in our calculations we find the change in the carrier density is no more than 30%.

As shown in Figure 2.1.13, $\Delta n/N$ increases by a factor of $\approx 2.5 - 3$ for $N \sim 10^{17}$ cm^{-3} as the MQW well size decrease from bulk to 47 A MQW. The linear absorption spectra for these samples show that the linear absorption coefficient α_0 is increased form bulk to 47 A MQW. The larger α_0 for the smaller well MQW results from the decrease in their Bohr radii, a_B (since the transition probability is proportional to $1/a_B^{-3}$). These results indicate that the factor of 2.5 to 3 increase in the optical nonlinearities are mainly due to the increase in the exciton absorption.

In summary, the systematic study of the dependence of the optical nonlinearities on well thickness for GaAs/AlGaAs MQWs and bulk GaAs at room temperature shows a ratio of nonlinear refractive index to carrier concentration increases by a factor of 2.5 to 3 as the well size decreases from bulk to 47 A. The increase in nonlinearity is due to larger absorption coefficient for smaller well sizes. However the larger absorption for the MQWs means that greater detunings must be used for device applications to avoid large absorption. This may explain the observation that the threshold power for optical bistability is nearly constant for both MQWs and bulk. We note that the larger nonlinearity and the better compatibility with existing semiconductor lasers tends to favor MQWs over bulk GaAs for device applications. Futhermore, the pump-probe experimental nonlinear transmission

results agreed very well with the four-wave mixing results.

2.2 *Nonlinear Optical Properties of Doping (n-i-p-i) Superlattices*

Doping superlattices are periodic structures composed of thin, alternating n and p doped layers which may or may not be interspersed with undoped layers. In addition to their two-dimensional behavior, which they share with compositional superlattices, they exhibit novel optical and electrical effects. Absorption, refractive index and carrier lifetime can all be tuned by either electrical or optical injection of carriers. More significantly large optical nonlinearities are achieved with much lower powers than required in compositional superlattices.

Dohler first proposed the idea of a doping superlattice. In the nipi structure, the modulation in the doping through the sample leads to a space charge potential which modulates the conduction and valence bands (Figure 2.2.1). The built-in potential from the space charge creates an internal field which tends to spatially separate the electrons and holes. The reduced overlap of the electron and hole wavefunctions enhances the carrier lifetime by several orders of magnitude. The built-in electric field also changes the shaped of the absorption spectrum of the GaAs via the Franz-Keldysh effect. The Franz-Keldysh effect produces a uniform shift of the absorption edge to lower energy with an oscillating behavior for the absorption near the gap. Nonlinear optical effects in nipi structures are produced by injection of free carriers which tend to neutralize the built-in electric fields. Under low excitation, large numbers of carriers can be built up over time because the carrier lifetimes are so long. Under large excitation the conduction and valence bands "flatten" and become more bulk-like. This reduces the recombination time of the electrons and holes and reduces the Franz-Keldysh absorption effects below the gap.

Reducing the optical power threshold for nonlinear action is desirable in certain optical device applications, especially for dense arrays of switching pixels. Because of the long carrier lifetime achievable in doping superlattices, it might be possible to integrate over time the carriers produced by a low power control beam and effectively trade-off low power operation with long lifetime response.

The concepts applicable to doping superlattices can be readily extended to

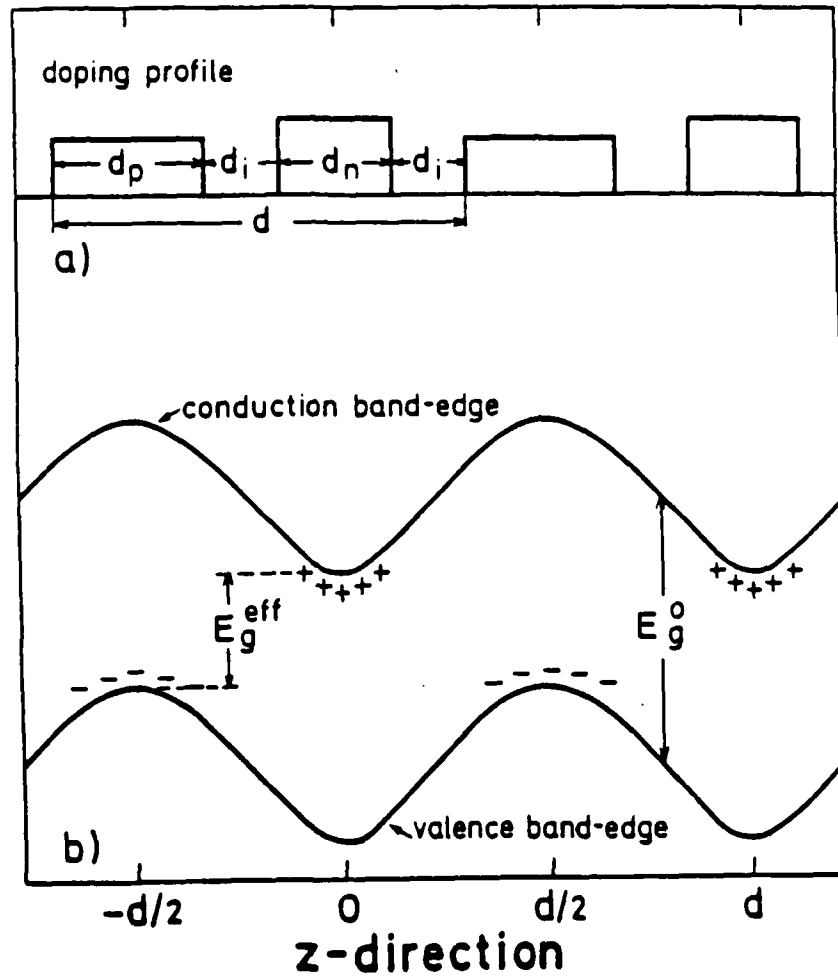# Schematic Doping Profile and Band Diagram of NIPI Superlattice

Figure 2.2.1

structures that contain a periodic modulation of their chemical composition (heterostructures) in addition to the modulation in doping levels. In this program the so-called type II hetero-doping superlattices were investigated. The type II structures are composed of AlGaAs n-p multilayers with undoped GaAs quantum well layers interspersed between the n- and p- type doped layers. While retaining the tunability of the optical properties of doping superlattices, these structures allow the investigation of optical nonlinearities without the deleterious broadening effects associated with heavy doping.

To study the nonlinear optical effects in GaAs/AlGaAs doping superlattices 10 samples were grown, seven of which were homo-nipis (homogeneous host material) and three which were type II hetero-nipis (the intrinsic layers are undoped GaAs while the doped layers are AlGaAs). Two of the homo-nipis were incorporated within a superlattice mirror / Fabry-Perot structure. The design parameters of the ten samples are displayed in table 2.

Table 2a (homo-nipis).

sample	n-layer	p-layer	periods	comments
1028	GaAs 600Å 10^{18}/cc	GaAs 600Å 10^{18}/cc	30	MBE
1229	GaAs 1300Å 2×10^{17}/cc	GaAs 1300Å 2×10^{17}/cc	10	MOCVD
1230	GaAs 1300Å 2×10^{17}/cc	GaAs 1300Å 2×10^{17}/cc	10	MOCVD
1236	same as 1230			
mh50	GaAs 500Å 1.3×10^{18}/cc	GaAs 370Å 1.77×10^{18}/cc	12	{λ/4 stack cavity 870nm center MOCVD}
mh51	same as mh50			
mh52	GaAs 550Å 1.3×10^{18}/cc	GaAs 400Å 1.77×10^{18}/cc	11	{λ/4 stack cavity 870nm center MOCVD}

sample	n-layer	i-layer	p-layer	i-layer	periods	comments
mh40	360Å 0.5-4x10^{18}	270Å 10^{15}	345Å 1.1x10^{18}	600Å 10^{15}	10	MOCVD
mh41	360Å 0.5-4x10^{18}	350Å 10^{15}	360Å 10^{18}	350Å 10^{15}	10	MOCVD
1273	200Å 3.1x10^{18}	100Å	238Å 2.6x10^{18}	100Å	12	MBE

Material Characterization

As part of the growth process, doping levels and layer thicknesses were measured using Hall and SEM techniques respectively. Hall measurements also provided carrier mobility information which was useful in indicating the purity and quality of the material. Calibration layers would be grown by MOCVD or MBE than characterized using these tools before the final sample was grown.

Photoluminescence was used as the primary material characterization technique for the doping superlattices. Using excitation intensity dependent photoluminescence, the shift in the band energy was measured. Under high excitation the material emitted a peak close to that of bulk while under lower excitation that peak would shift to longer wavelengths. Figure 2.2.2 depicts this process. Generally these measurements were made at a sample temperature of 77K using an Ar+ (514.5 nm) or a HeNe (632.8 nm) laser as the excitation source.

Linear absorption spectroscopy was also a very important tool used to measure the optical absorption spectra of the material. Before these measurements could be made the GaAs substrate was etched off using the same method as described

Photoluminescence Spectra from a Doping SL for Different Excitations

DSL 1182   T = 77K λ_{exc} = 514.5nm

A I_{exc} = 100 w/cm^2

B I_{exc} = 10 w/cm^2

C I_{exc} = 0.55 w/cm^2

D I_{exc} = 0.02 w/cm^2

0.8   0.9   1.0
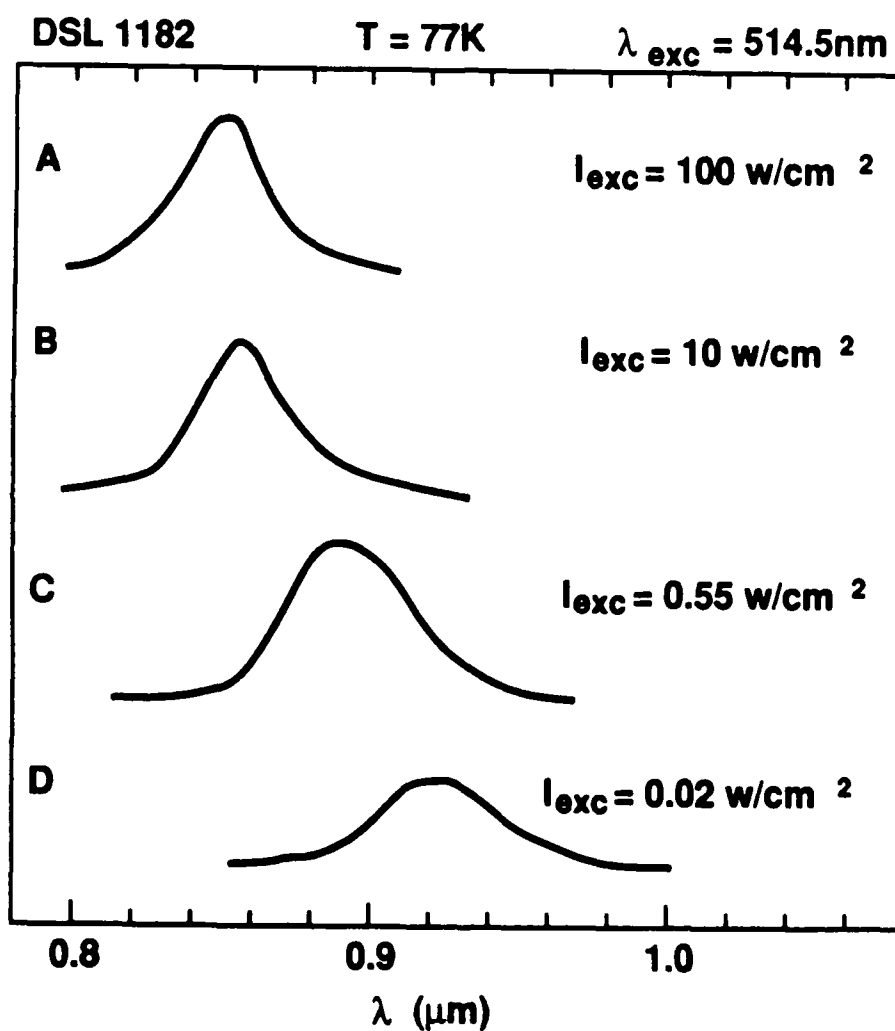
λ (μm)

Figure 2.2.2   Intensity dependent photoluminescence spectra.

earlier in this report. Sapphire substrates were used as mechanical supports. The measurements were made by two techniques. A Perkin-Elmer Dual Beam UV-Vis-IR spectrometer provided us with transmission and reflection spectra which was converted to an absorption spectra. A figure showing a plot from this system is shown in Figure 2.2.3. The other technique used the same setup that was used for the nonlinear transmission measurements. A broad-band (770nm-900nm) low power beam was focused onto a sample with the reflection and transmission being collected and analyzed with a spectrometer. Both techniques were useful in describing the absorption properties of the nipi superlattice.

Nonlinear Optical Measurements

The experimental technique we used for determining the nonlinear properties in GaAs/AlGaAs nipi superlattice was the nonlinear transmission measurement which is diagramed in figure 2.2.4. The spontaneous luminescence from an Argon-ion laser pumped dye laser was used as the probe beam and was collected and focused onto the sample. The dye was Stryrl 9 and provided a broadband beam from 770nm-900nm. The probe beam power was kept low so as not to excite the system. The pump beam was either a HeNe laser or an AlGaAs diode laser. The transmitted probe beam was analyzed by a Jarrell-Ash 0.5 meter spectrometer with a GaAs photomultiplier detecting the output. The GaAs photomultiplier had a useful range to about 900nm thus only a small energy range below the GaAs bulk band gap could be covered when the sample was at room temperature. An optical chopper was used in conjunction with a lock-in amplifier to improve the signal to noise ratio. If the nonlinear transmission was being measured than the chopper was placed in the pump beam path. If the linear transmission was being measured than the chopper was placed in the probe beam path. The output of the lock-in amplifier was acquired by a PC using as A-D converter. Once on the PC the data could be stored, analyzed and plotted.

Typical spectra of the percentage change in transmission vs. photon energy for different excitation levels is shown in figure 2.2.5. Using the ratio of these spectra the following expression was used to arrive at a $\Delta\alpha$ spectra:
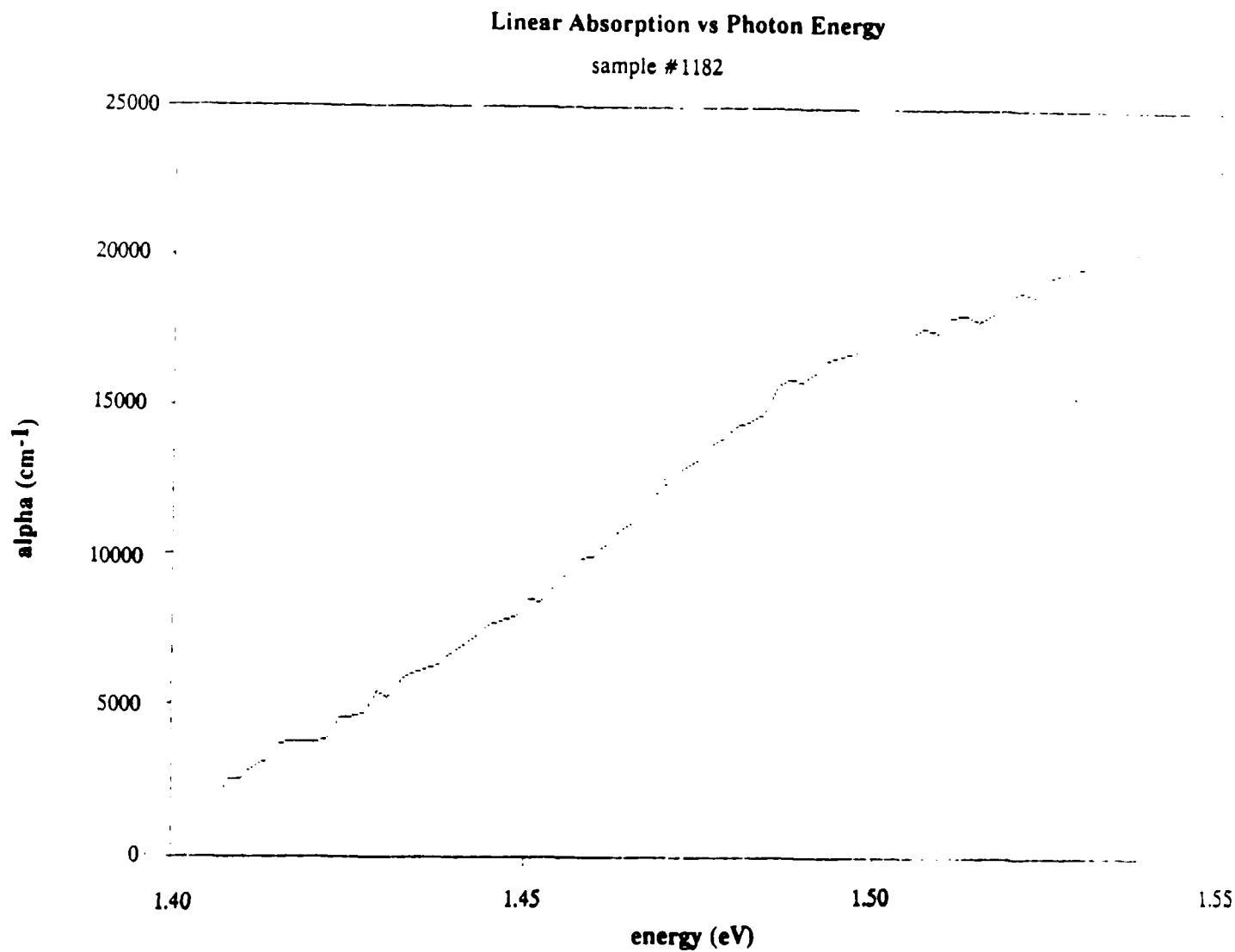
Figure 2.2.3   A plot of linear absorption for a GaAs doping superlattice.

Nonlinear Optical Transmission Experimental Setup

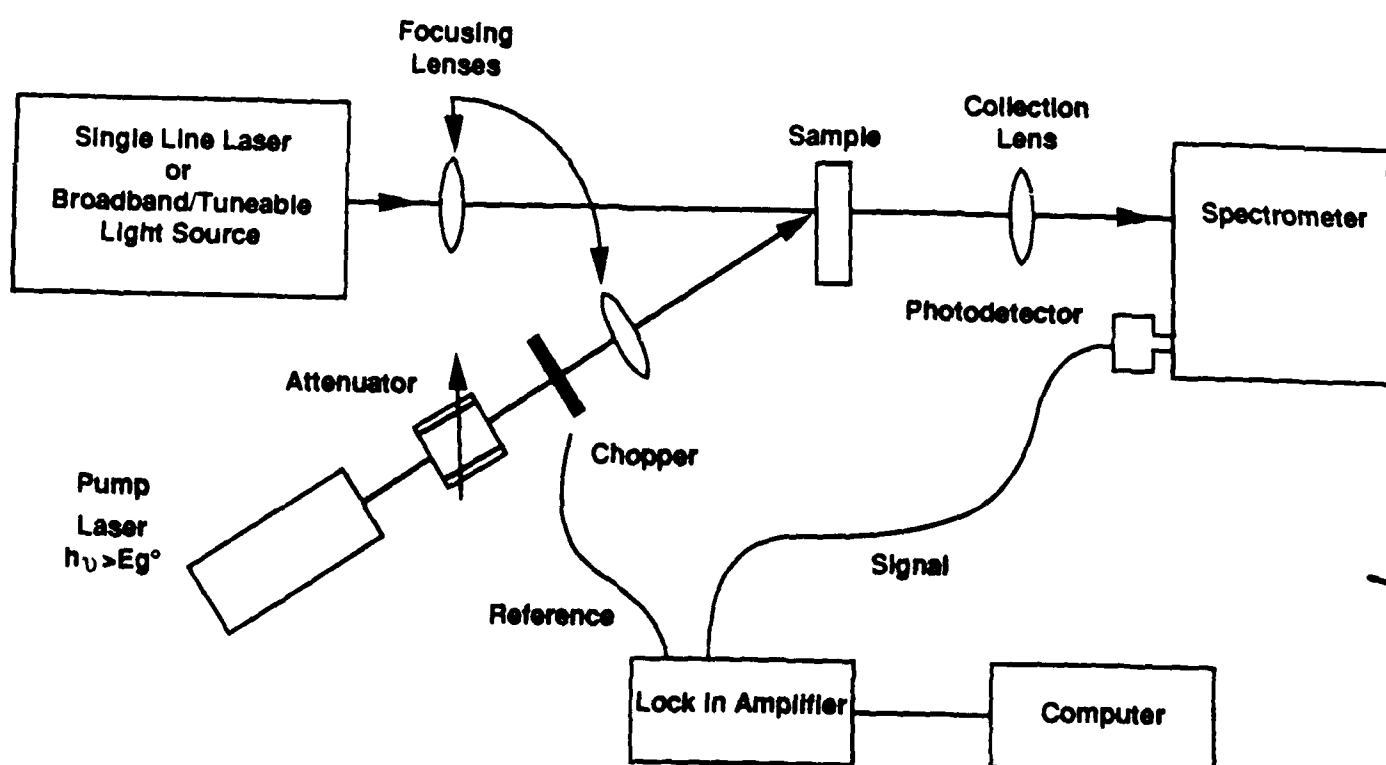Figure 2.2.4

Optically Modulated Transmission
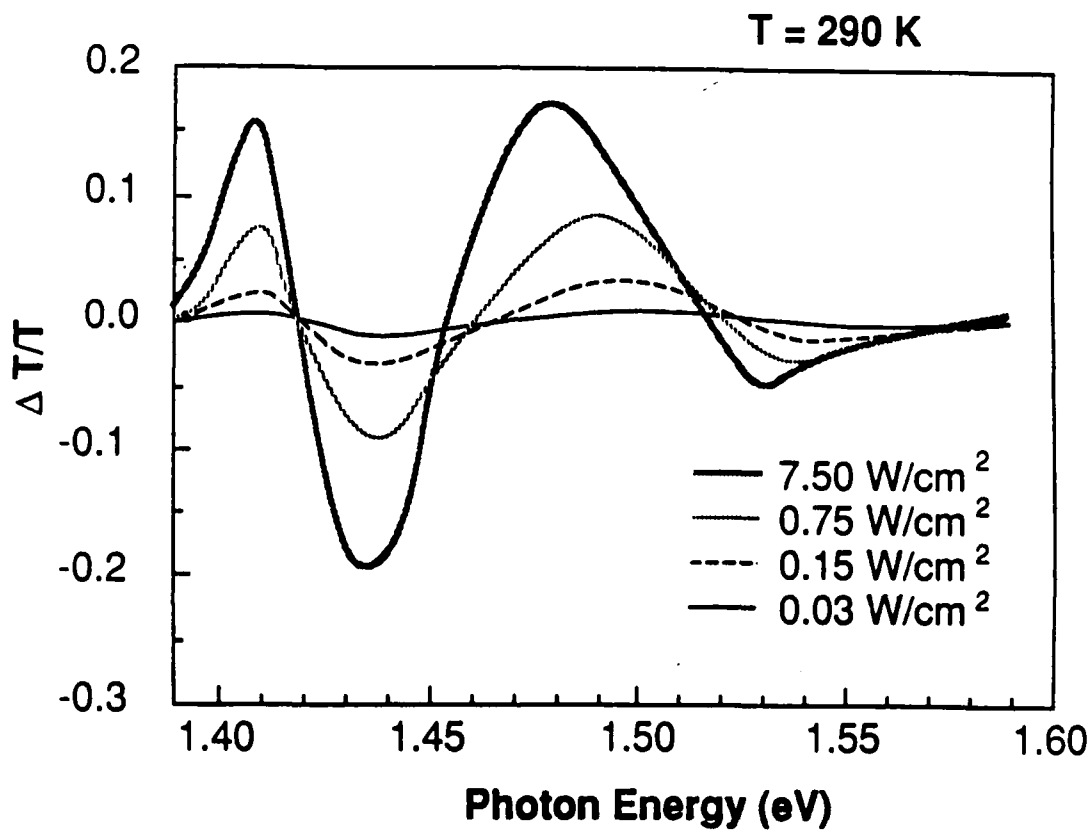## in GaAs Doping SL for different excitation levels

T = 290 K

Legend:
- 7.50 W/cm^2
- 0.75 W/cm^2
- 0.15 W/cm^2
- 0.03 W/cm^2

Y-axis: $\Delta T/T$

X-axis: Photon Energy (eV)

Figure 2.2.5

$$\Delta\alpha = -l^{-1} \ln[1 + \Delta T/T], \qquad\qquad (5)$$

where l = sample thickness (GaAs). A $\Delta\alpha$ vs photon energy spectra is shown in figure 2.2.6. The increase in the transmission below the band gap is due to the decrease in the internal electric field strength associated with the excitation of carriers and the resulting decrease in the tunneling assisted Franz-Keldysh absorption. Near the gap the transmission decreases which is attributed to band-gap shrinkage and the undepleted central regions of the p-layers with increasing charge carrier population. Band shrinkage effects in the n-layers are partially counteracted by the Burstein-Moss shift associated with band filling. The Burstein-Moss shift is expected to be negligible in the p-layers due to the large hole mass. The oscillatory behavior at larger photon energies is attributed to Franz-Keldysh oscillations.

Using the Kramers-Kronig relation one can arrive at a spectra of the change in index starting from the absorption change spectra. The Kramers-Kronig relation is given by the following:

$$\Delta n = ch/2\pi^2 \ P\!\int E'\Delta\alpha(E')dE'/[(E')^2 - E^2], \qquad\qquad (6)$$

A calculated delta n spectra is shown in Figure 2.2.7.

Degenerate Four-Wave Mixing in Doping Superlattices

To verify that the calculated delta n spectra were accurate, degenerate four-wave mixing (DFWM) was done. In combination with delta alpha measurements, DFWM would allow an alternative to the Kramers-Kronig calculation in arriving at a delta n spectra. The experimental setup was the same as the one described in Figure
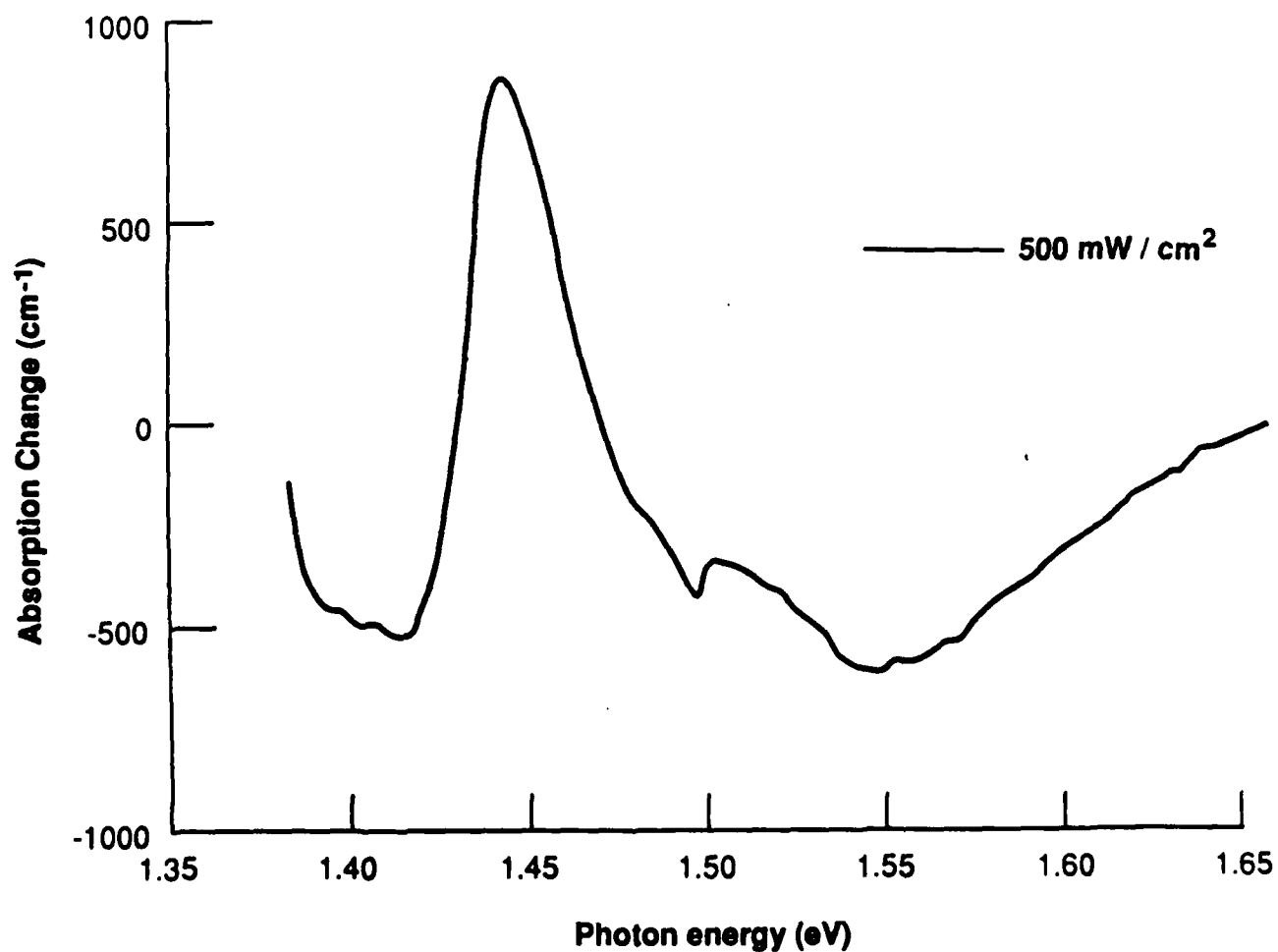
Absorption Change in GaAs Hetrero-nipi

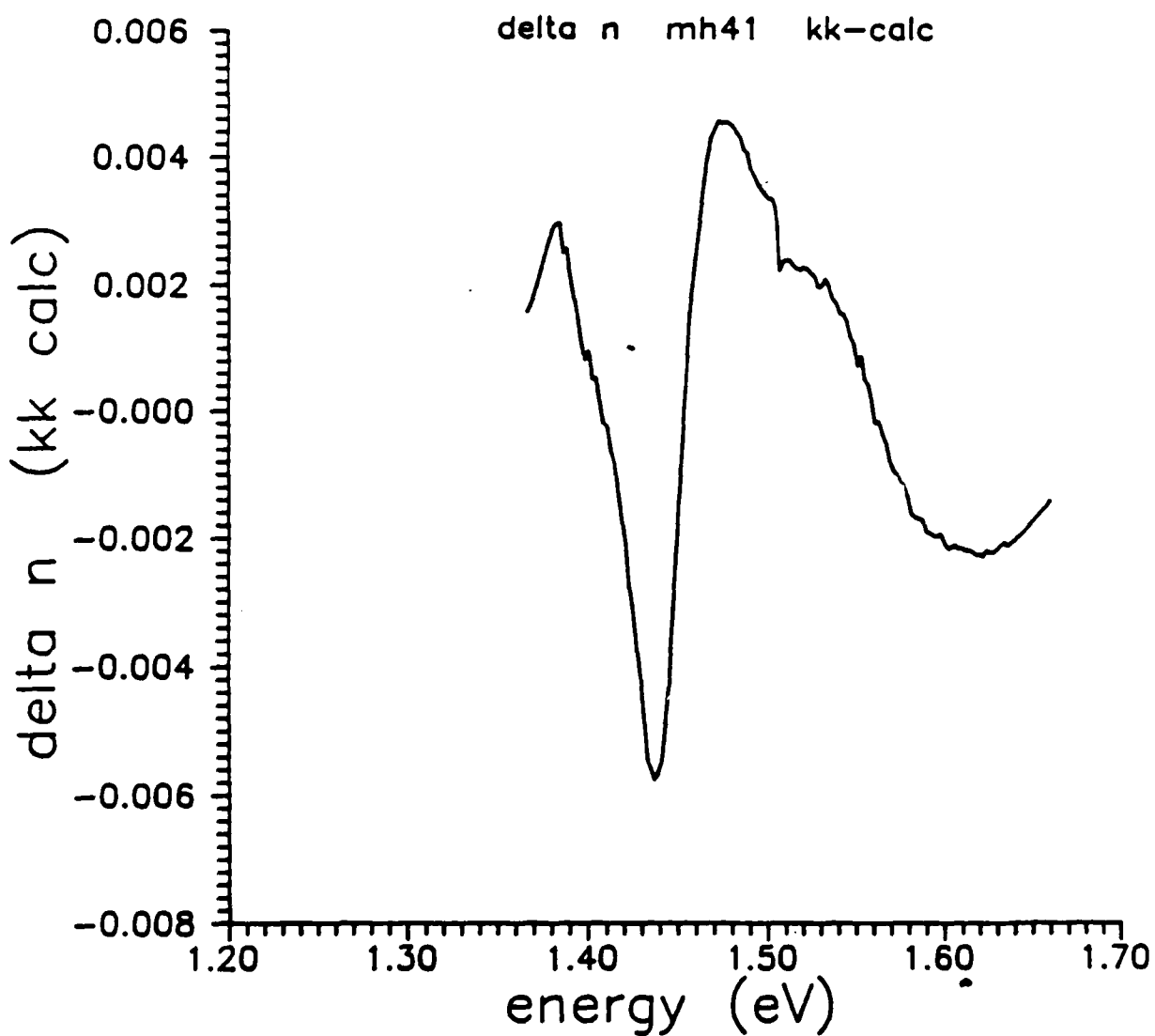Figure 2.2.6   Absorption Change ($\Delta\alpha$) in a GaAs Hetero-Doping Superlattice

Figure 2.2.7   Kramers-Kronig calculation of the index change of a GaAs Hetero-Doping
Superlattice.

39

2.1.5. Before the measurement was made, the signal was simulated using the $\Delta\alpha$ and the Δn results obtained by nonlinear transmission spectroscopy and Kramers-Kronig transformations. The diffraction efficiency is given by the following equation:

$$\rho_s \approx [(2\pi\,\Delta n/\lambda)^2 \; + \; (\Delta\alpha)^2](l/2)^2 \exp(-\alpha l) \tag{7}$$

However it was found that the experimental values for the diffraction efficiency were roughly two orders of magnitude less than expected from the simulation. This can be accounted for by remembering that the doping superlattices at a low power excitation has very long carrier recombination times. Assuming that the ambipolar diffusion coefficient is 10 cm^2/s and the lifetimes are on the order of 10 μs than the diffusion length is $\sqrt{(D\tau)} = 10^{-2}$ cm. The grating spacing is given by:

$$\lambda = \lambda/2n \sin(\theta/2) = 1.07\,\mu m \tag{8}$$

where λ = 870nm, n = 3.5, and θ = 13°. After the first pulse the excited carriers diffuse and wash out the grating so that the diffraction efficiency is low. Because laser pulses have a 12ns period, the carriers don't fully recombine between pulses.

It was discovered late in the program that due to the very long diffusion lengths (~ 1mm), carriers excited by a focused light source will diffuse uniformly across the surface of the sample. This reduces the number of free carriers available to alter the nonlinear optical properties. Effectively this decreases the incident power needed to induce a large nonlinear effect. For example, a 1 W/cm^2 pump beam focused to a spot size of 1×10^{-3} cm^2 will excite carriers which will diffuse across a 1 cm^2 area thereby reducing the number of carriers at the focused spot by 1000x. Another way of looking at this effect is that if the carriers can be confined to the area being probed then it requires only 1 mW/cm^2 to induce large nonlinear optical effects. (This above discussion was not considered when the

40

nonlinear optical measurements were made).

University of Arizona Consulting Results

The research on doping superlattices at the University of Arizona under this program concentrated on the lifetime effects of the carriers. Although doping superlattices can have long lifetimes under low power conditions, to be useful in a device it must simultaneously maintain a long carrier lifetime and produce large absorptive and refractive changer. Both the nonlinear transmission and the nonlinear transmission modulation of a nipi structure were measured as a function of the incident intensity.

One of the structures examined by the University of Arizona was sample # 1229. In the experiment they directly measured the nonlinear transmission changes through the sample by a pump/probe technique. The pump beam from a cw dye laser was tuned to a wavelength (800nm) above the bandgap of the GaAs for efficient generation of free carriers. The pump and a broadband probe were synchronously modulated by acousto-optic modulators; the pump and probe pulse widths were 100 and 1 microseconds respectively. The separation time between pump pulses (typically 300 microseconds) was chosen so that the excess carriers have a chance to decay. The arrival time of the probe pulse relative to the rising edge of the pump pulse can vary continuously, even probing times after the pump is turned off. The probe passed through the sample under different pumping intensities and time delays and was collected by the optical multichannel analyzer (OMA).

The linear absorption spectrum of the sample is shown in Figure 2.2.8. The absorption bandedge is significantly broadened relative to bulk and the band tail extends to the long wavelengths, consistent with the Franz-Keldysh effect. The subband structure is not observable because of the strong broadening of the subband levels. The differential transmission spectrum ($\Delta T/T$) at various pump intensities is shown in Figure 2.2.9. As photocarriers accumulate and neutralize the space charge, the internal electric fields are suppressed, and the absorption edge pivots to sharper slopes. This enhances the transmission at long wavelengths
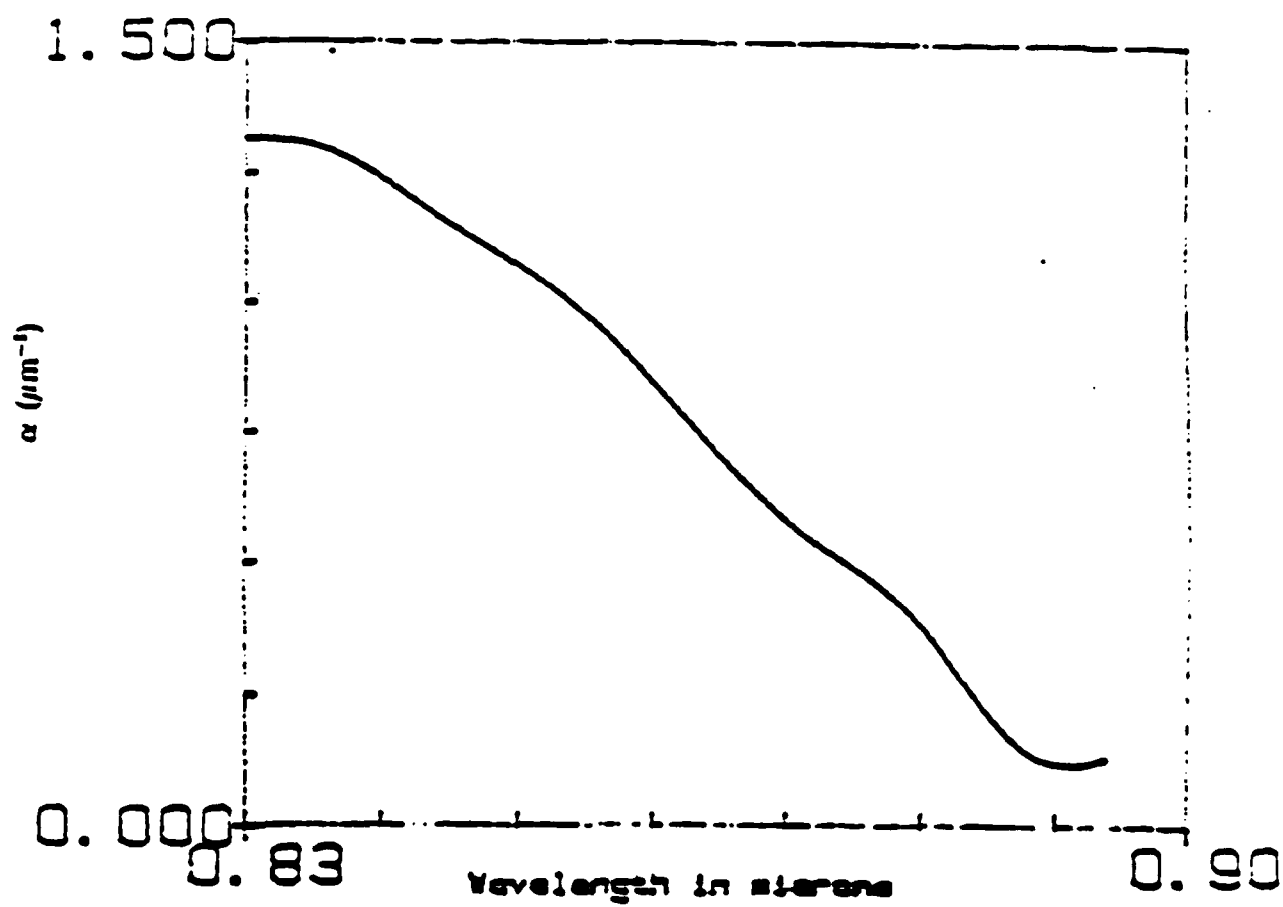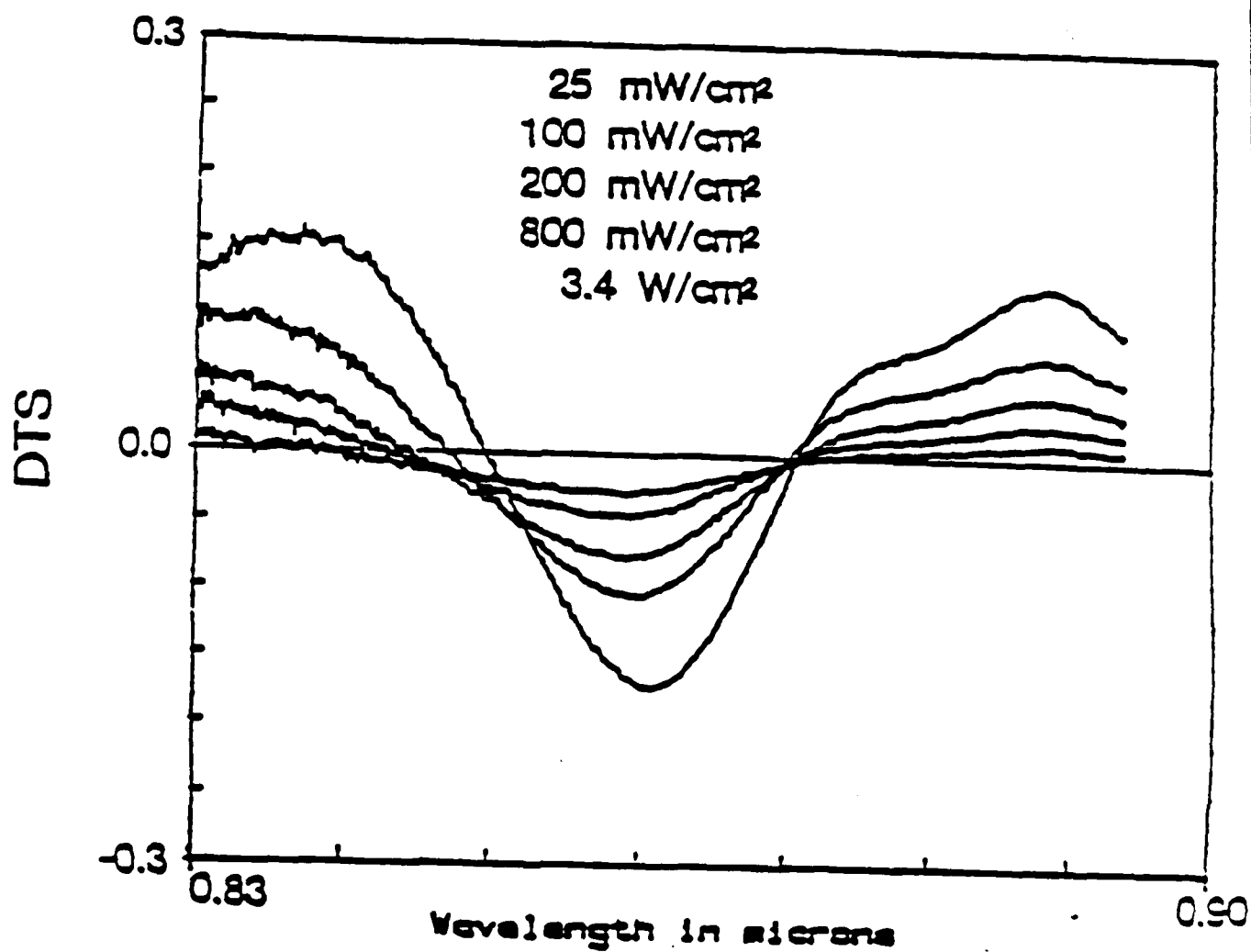
41

Figure 2.2.8

42

Figure 2.2.9   Differential transmission spectra $\Delta T/T$ at room temperature for different pump intensity values. The intensity values from highest to lowest are 3.4 W/cm^2, 800 mW/cm^2, 200 mW/cm^2, 100 mW/cm^2, and 25 mW/cm^2.

43

while increasing the absorption in the bandedge region. Figure 2.2.10(a) shows the build-up time required to obtain the maximum modulation for a given intensity. For the higher intensity (12 W/cm^2) the maximum modulation reaches steady state in 3 microseconds. However, this build-up time is increased to 40 microseconds for a lower intensity (1.2 W/cm^2) pump. This lifetime is three orders of magnitude longer than bulk. In general, increasing the injection rate (input intensity) by orders of magnitude does not change the carrier density proportionally nor at the same rate.

Intensity-dependent decay dynamics by delaying the probe relative to the falling edge of the pump were also measured. Both the build-up and decay dynamics can be effectively modelled with a rate equation whose carrier decay time depends exponentially on carrier density, N

$$dN/dt = -N/\tau(N) + \alpha(\omega)I/h\omega \qquad (9)$$

with

$$\tau(N) = \tau_0 \exp(-kN) \qquad (10)$$

where N is the carrier density, I is the intensity, $\alpha(\omega)$ is the absorption coefficient at the pump frequency, $h\omega$ is the photon energy, and $\tau(N)$ is the carrier-dependent lifetime. The numerical solution to this differential equation is shown in Figure 2.2.10b. The time dynamics of the carrier density build-up agree with the exponential curves. This density-dependent carrier lifetime is quite different from pure bulk or multiple quantum well GaAs and is part of the reason why nipi structures show large nonlinear effects with very low intensities.

In conclusion, we have investigated the nonlinear optical effects in GaAs Doping Superlattices and type II GaAs/AlGaAs Hetero-Doping Superlattices. We found that large nonlinearities are achievable at very low optical powers. In fact, as described above, due to diffusion effects not considered previously, the effective power to induce the nonlinear optical properties shown in the figures may be 1000x less. We feel that strong promise exists for future nonlinear optical devices based

44

on GaAs Doping Superlattices.

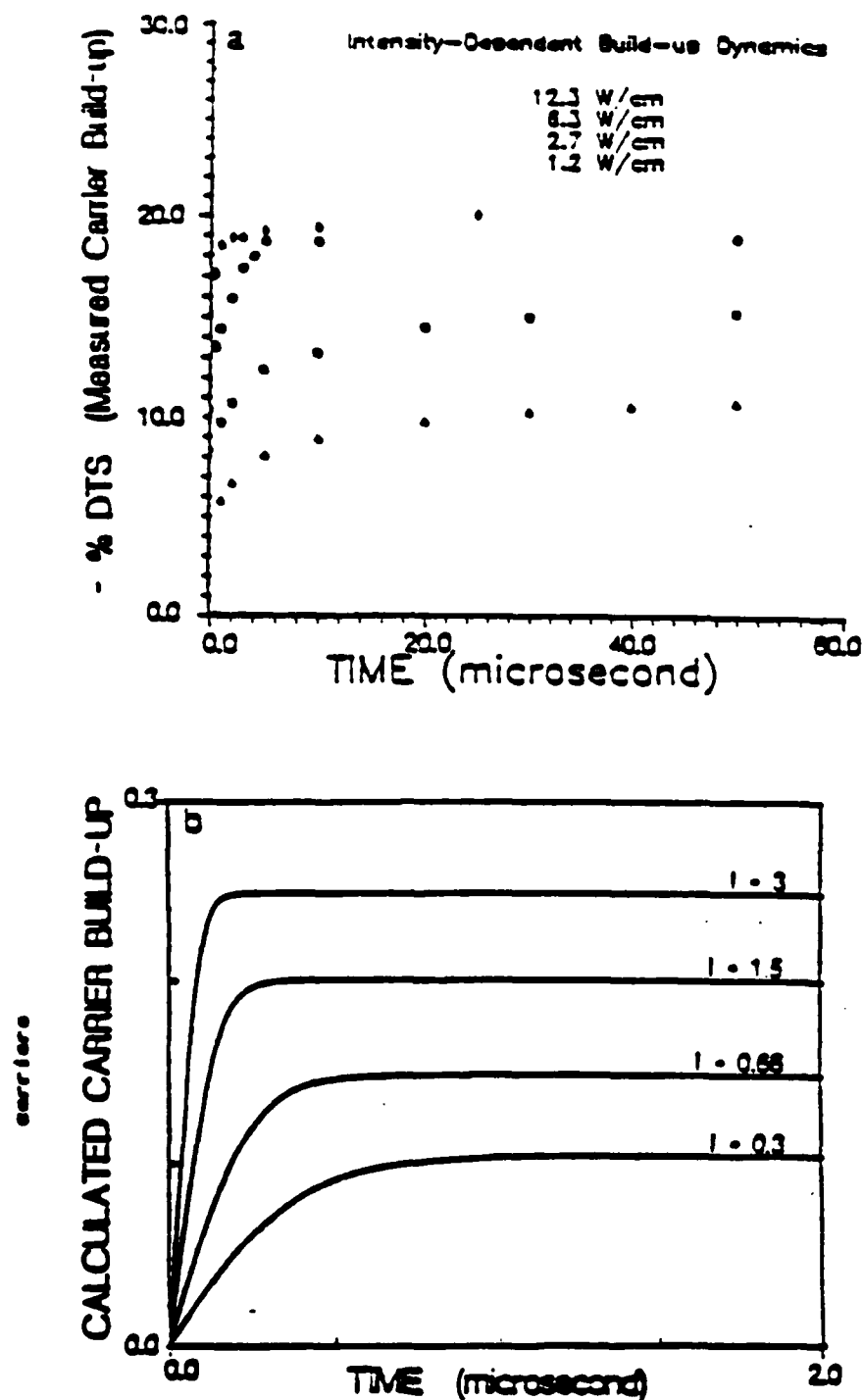Figure 2.2.10   intensity-dependent carrier build-up dynamics. (a) The maximum
                 modulation ΔT/T available at the given intensity is plotted as a function
                 of time. (b) The results from a rate equation model using a carrier-
                 dependent lifetime are plotted. $dN/dt = -N/\tau(N) + 1$; $\tau(N) = \tau_0 = 1$, k
                 = 10, and I = (3, 1.5, 0.66, and 0.3).

4.3 Low Power Light Modulation

An important motivation for doing this program was to develop a material system in which very large optical nonlinearities could be achieved at low powers and could potentially be used in a spatial light modulator design. Although the optical nonlinearities in the doping superlattice are large, the nonlinear transmission changes by only approximately 20% (0.97dB). However since this modulation occurs across only ~ 1 μm of material, the possibility exists that by increasing the optical path length, either by using a waveguide to travel along the layers or a Fabry-Perot cavity to make multiple passes, considerable enhancement of the extinction ratio could be obtained. In addition, the nonlinear effects are achieved at low power which is critical for the design of large arrays of elements.

The nipi structure is an ideal candidate for a multiple pass configuration. Doping Superlattices have large nonlinearities below the band edge where the absorption is low so that multiple passes through the nipi can be made to enhance the modulation without prohibitive degradation of the signal. The simplest design for this light modulator is based on a Fabry-Perot interferometer whose active medium consists of a doping superlattice. The nonlinearities in the refractive index and the absorption coefficient can then be used to alter the transmission characteristics of the resonant structure.

A computer code was developed which simulates the transmission properties of the doping superlattice resonant cavity. Models developed under this program which predict the behavior of the doping superlattice were used to determine the nonlinear optical parameters. The Fabry-Perot transmission was derived in "Principals of Optics" by Born and Wolf. Figure 2.3.1 shows a calculated result of the transmission characteristics for a 5 micron thick doping superlattice surrounded by 90% and 98% reflective mirrors. Our model predicts that depending on the reflectivity of the mirrors, a 15 to 27 dB extinction ratio can be expected. The change in transmission amplitude is due to the large change in absorption near the band edge. The small shift between the two transmission states is due to the index change. Obviously the absorption plays a more important role in the transmission modulation near the band edge (~ 1.42 eV). Properly optimizing the device includes designing the cavity thickness such that a cavity resonance occurs
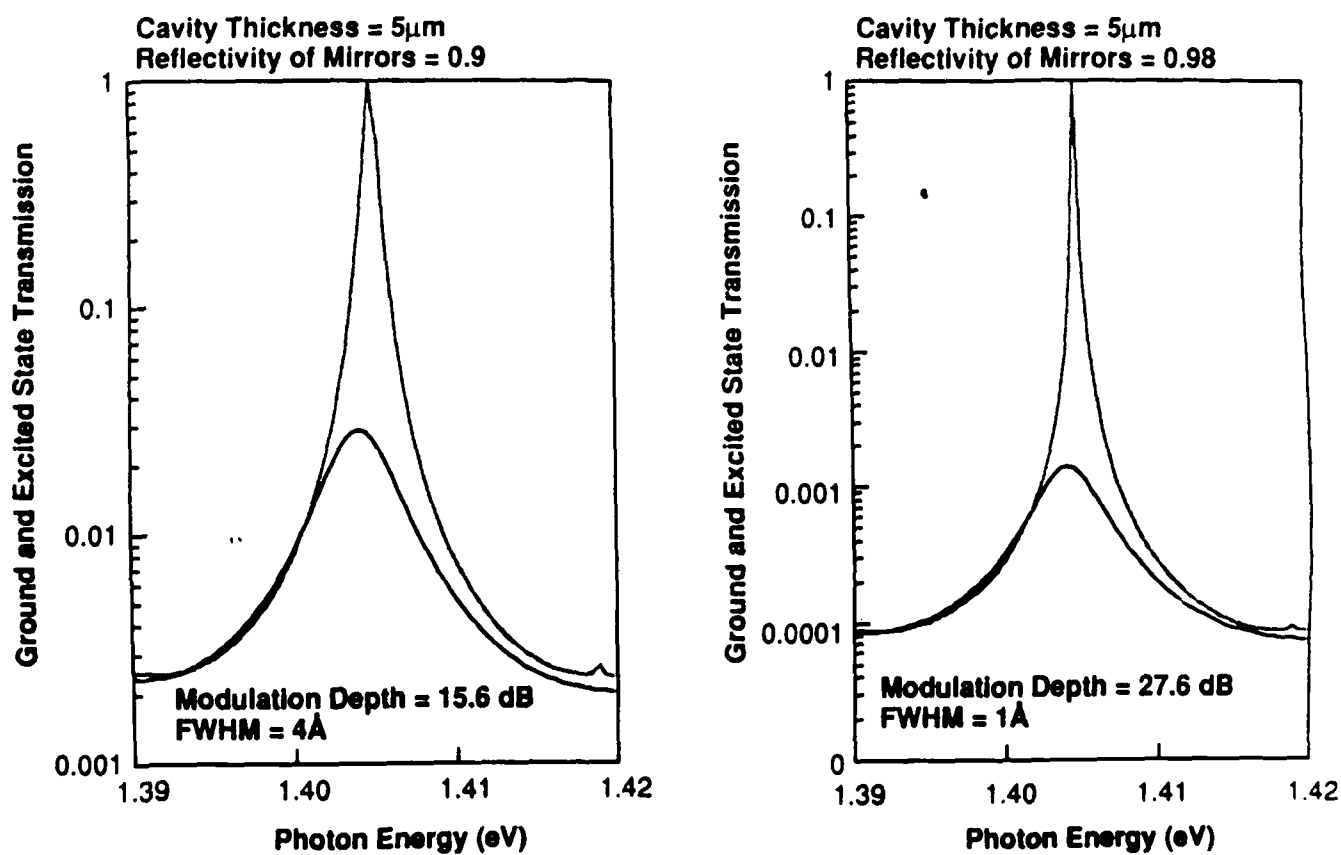
Fabry-Perot Transmission for GaAs nipi

Figure 2.3.1   Doping Superlattice resonant cavity transmission calculations.

48

at the greatest absorption change.

To demonstrate this concept samples mh50, mh51, and mh52 were grown (table 2a). These unoptimized samples had 1.04 μm of active material (nipi) sandwitched between two GaAs/AlAs $\lambda/4$ stack superlattice mirrors. The epitaxial growth was performed by MOCVD. The structure was mounted on a sapphire disk and the GaAs substrate was chemically etched off using the method described earlier. Figure 2.3.2 shows a diagram of the structure. The mirrors, which were developed under a Honeywell corporate program, were of high quality reflecting more than 90% at the center wavelength. Figure 2.3.3 shows a reflection spectrum of one of the mirrors. Just as in a dielectric mirror, the center wavelength of the reflection spectrum can be tuned by changing the thicknesses of the GaAs and AlAs layers so that the maximum reflectivity is placed where the nipi properties are most promising.

These structures were characterized using the nonlinear transmission experimental set-up illustrated in Figure 2.2.4. A 1 W/cm^2 HeNe beam was used as a pump. A change in transmission of 40% through the cavity structure was measured. This is a 4x increase in the transmission change that was measured from a comparable doping superlattice without the mirrors. Analysis of the reflectivity properties of the mirrors surrounding the doping superlattice showed that the mirror between the doping superlattice and the GaAs substrate had a center wavelength reflectivity that was shifted away from the design value. This means that the resonating properties of the cavity were poor and contributed to the lower than expected change in transmission. By proper optimization of this structure, extinction ratios approaching the predicted values could be obtained.

Resonator Structure

AlAs/GaAs Quarterwave Mirror	GaAs	$\lambda/4$
	AlAs	$\lambda/4$
	GaAs	$\lambda/4$
	AlAs	$\lambda/4$
	GaAs	$\lambda/4$
	AlAs	$\lambda/4$

GaAs/AlGaAs Hetero-nipi

p-AlGaAs
i-GaAs
n-AlGaAs
i-GaAs

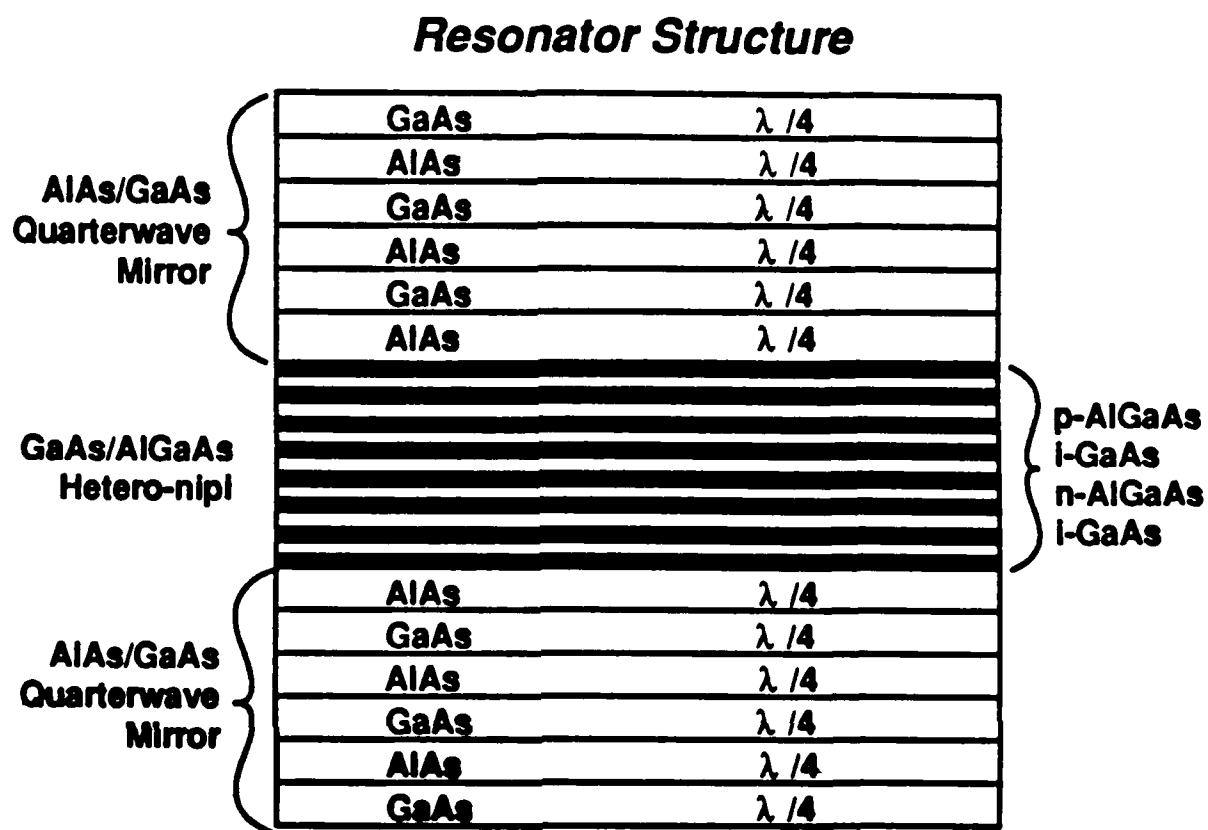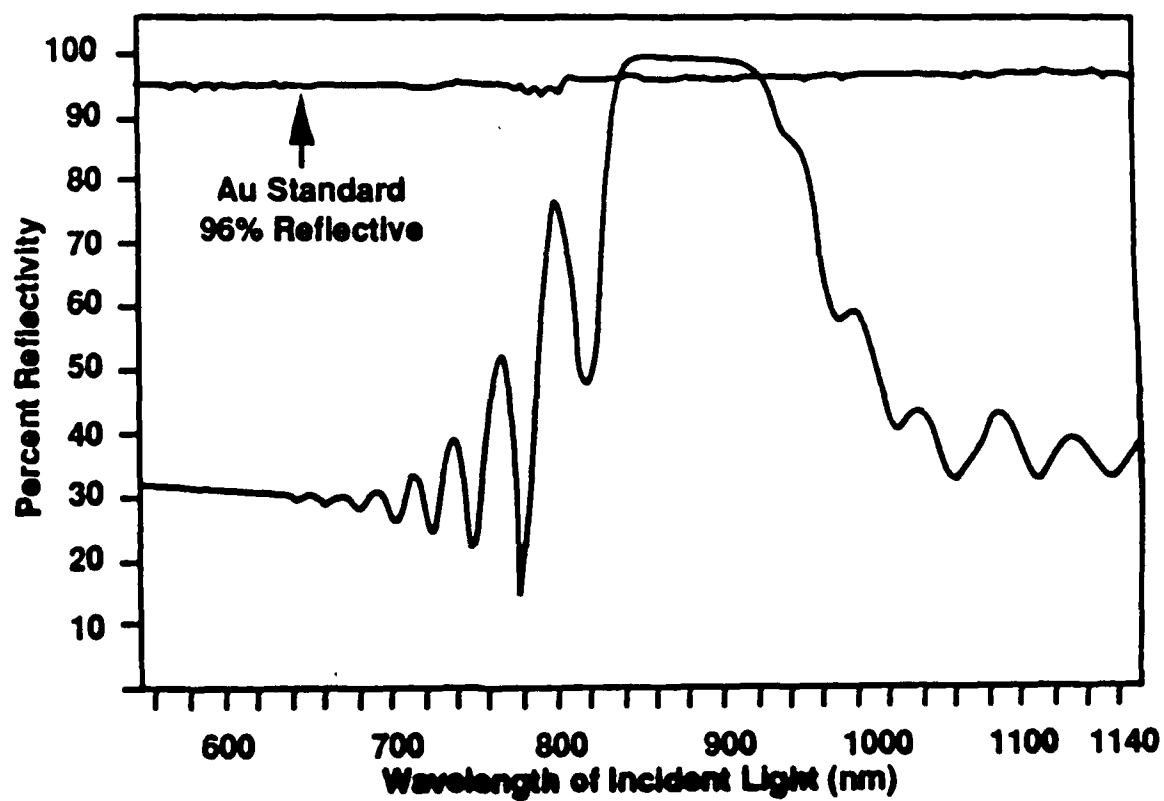| AlAs/GaAs Quarterwave Mirror | AlAs | $\lambda/4$ |
	GaAs	$\lambda/4$
	AlAs	$\lambda/4$
	GaAs	$\lambda/4$
	AlAs	$\lambda/4$
	GaAs	$\lambda/4$

Figure 2.3.2   Schematic of the resonator structure grown by MOCVD.

Figure 2.3.3   Reflectivity spectrum of a 40 period AlAs/GaAs Superlattice Mirror.

Spatial Light Modulator Applications

Introduction

This report summarizes the most significant applications of spatial light modulators, and outlines the performance required of the modulators in each application. Particular attention is given to the use of nipi type structures in the candidate architectures, and the resulting performance compared against that arising from the use of other types of modulators.

Spatial light modulators are generally most appropriate for free-space based systems, although in a few situations their properties are compatible with guided-wave systems. The principal areas of application considered here are:

1) Optical interconnection

2) Incoherent-to-coherent conversion

3) Neural networks- associative memories and others

4) Correlators

5) Displays

6) Spectrum analysis

8) Optical and Optoelectronic Logic

SLM Alternatives

In considering the incorporation of nipi based SLMs in the target systems, some comparison with other SLM technologies is important. The performance and characteristics of current SLMs will therefore now be described. For a more detailed discussion of the properties of the various devices the reader is referred to references 1 and 2. Both optically and electrically addressed SLMs are of interest for optical systems, and will be considered here.

Liquid crystal SLMs

Nematic liquid crystals may be used in an analogue polarization rotation scheme, requiring drive voltages of some tens of volts (3), and having relatively low speed,

typically 1kHz. Optically addressable spatial light modulators have been demonstrated by integrating a bulk single-crystal $Bi_{12}SiO_{20}$ photoconductor (2). The device allows for different read and write wavelengths, thus operation at the read wavelength should not affect the stored modulation. Resolutions obtained for such a structure are 10 line-pairs/mm for a 15um thick liquid crystal layer. The resolution will obviously increase as the thickness is reduced. Surface areas of one square inch have been demonstrated. The Hughes liquid-crystal SLM operates in a similar manner, but operates in a reflective mode, thus enabling reading and writing to occur at the same wavelength, without mutual destruction.

Ferroelectric liquid crystals have shown extinction ratios as high as 50db, with speeds up to 10MHz. The operation of these crystals has to date been digital, ie. only two transmission states are possible. Smectic A liquid crystals are expected to exhibit analogue behavior, but without the hysteresis characteristic of the current smectic C devices.

PLZT SLMs

By application of a voltage of some hundreds of volts to a PLZT wafer in a transverse direction, the device transmission can be modified from opaque to transparent. Land (4) has demonstrated contrast ratios of 300:1 (24dB) with resolutions of 40 line-pairs/mm. Obvious disadvantages are the high drive voltage, and the implicit limitation to speed due to the finite slew rate of available electronics. PLZT has also been used in a photosensitive mode to achieve a deformation of a wafer dependent upon the incident intensity (12).

Microchannel Plate SLMs developed by MIT integrate photocathodes with a microchannel plate array, converting an incoherent of coherent illumination to a voltage applied to a lithium niobate plate. This allows the state of polarization of light incident from the other side of the plate to be rotated, hence allowing amplitude modulation. Typical write times are 50ms, while erasure requires 100ms. Resolutions are lower than many other modulators at 5 line pairs/mm due to spreading of the charge in the plate.

Deformable mirrors developed by Texas instruments are etched silicon structures in which either optical or electrical addressing is used to displace a thin membrane, thereby imparting a combination of phase and intensity modulation to light reflecting from the array. Response times of 25 microseconds are common, while the pixel size is 25 x 25 microns. Operating voltages are typically 30 Volts. Resolutions obtained have been 20 line-pairs/mm.

Pockels read-out modulators are high-voltage devices (1-2kV). Modulation is effected by using short wavelength light to generate carriers in a photorefractive crystal, which then cancel out an applied field, resulting in a variation of crystal birefringence with position (5,11). Typical resolutions obtained for a 1mm plate are 40 line pairs/mm. A useful feature of these devices is the ability to modify in real time the contrast of the modulator by application of an electric field. This results in the ability to add or subtract an amplitude term to all pixels, thus aiding some signal processing functions.

Magneto-optic Spatial Light Modulators rely on magnetization of a small area of a magnetooptic modulator sheet by current flowing through two intersecting conductors. By ion-implanting a small region of each pixel, selective addressing of the modulators is accomplished. The magnetization remains after removal of the initiating current, thus

addressing of an entire array is possible. The induced magnetization results in a rotation of the polarization of a few degrees for light propagating through the thickness of the modulator. Disadvantages to this device are the low efficiencies.

Each of the above modulators represents a tradeoff of some properties against others. For example, high extinction ratio devices are generally incompatible with high speeds of operation. Parameters of concern for system application include:

(i) Required drive voltage for electrical addressing, or   sensitivity for optical addressing
(ii) Extinction ratio (ratio of maximum to minimum transmission)
(iii) Response time
(iv) Spatial resolution

Strengths of the nipi lie in the controllable lifetime, and the high extinction ratio attainable from resonant structures incorporating nipis. Drive voltages are also lower than some other electrically addressed SLMs. The high sensitivity attainable for optically addressed spatial light modulators. Weaknesses include the limited device operating speed, dictated by slow recombination in the erase mode, and by the narrow wavelength range within which high extinction can occur.

1. Optical Interconnection

Spatial light modulators have been used for generalized crossbars in both free-space and guided-wave implementations. Their application to interconnection is severely limited due to inherent losses in the architecture. However, it is relatively easy to implement functionality such as full broadcast which are harder in guided wave optoelectronic versions. Optivision's crossbar is an example of such a system, based on vector-matrix multiplication. Figure 1 shows the arrangement. An output O_j is given by the sum of all possible row inputs multiplied by the weights in each pixel of the mask, or:

$$O_j = \Sigma \; w_{ij} I1.$$

Where I and O are input intensities for incoherent illumination, or a coherent sum of fields for coherent illumination.

Speed required for reconfiguration depend on the application, but for comparison, guided-wave optoelectronic versions could reconfigure in one nanosecond, once all controlling voltages had been derived. In any vector-matrix based system, extinction ratio of the individual elements is of concern. Suppose that all input elements were fully illuminated, but that only one column of the matrix was intended to transmit. Summing across a row, we would find that one element had an output of T^o_n, while (N-1) elements would have a transmission of T_{off}. Thus the signal-to-noise ratio would be $T_{on}/(N-1)T_{off}$, which for large N simply becomes the device extinction ratio divided by the linear dimension of the array. Thus a 100 x 100 array would require an extinction ratio of 40dB for a signal-to-nose ratio of 20dB. Alternatively, an extinction ratio of 25dB implies that only a 4 x 4 matrix could be used with a received extinction ratio of 20dB. We note that this simplistic analysis has ignored compensation possible for the non-linear transfer function resulting from a known finite extinction ratio.

The free-space crossbar based on vector-matrix multiplication enables broadcast to be implemented with ease: this is not possible for many other types of crossbar. The inherent masking operation of the crossbar results in an intrinsic loss of 3dB for a 2 x 2, increasing to 12dB for a 16 x 16 crossbar. In addition, considerable loss is experienced in combining the signals at the output of the crossbar, if space occupied by each output is not to be proportionately larger than the inputs. Alternatively, if for example the crossbar were interfaced to multimode optical fibers, when all outputs of a column were summed using a fiber coupler, the diameter of the output fiber would need to be a factor of N larger than each input, numerical aperture remaining constant. Thus the use of SLMs for crossbars is unattractive for scalable designs.

The ferroelectric liquid crystals, with high extinction ratio and low drive voltage, coupled with high speed, would appear to be the most appropriate choice. However, our discussion has centered on electrically addressed SLMs. Since an N x N crossbar would require N^2 electrical lines, it may be advantageous in some applications to generate the required weights via a vector outer product, and transfer this information to the interconnection weight matrix. It would be in such architectures that the NiPis may find application for interconnection. The strength of using them is this application would lie in a higher optical sensitivity than competing techniques. The nipi weight matrix would need to be updated only when the matrix element values were to be altered. However, the weight matrix may need to updated more often than desired. The finite lifetime of the excited nipis results in the requirement of periodic refreshing. Of more concern however is the degradation of the "off" state of the elements which would result from absorption of the incident radiation at those pixels. The high fanout and fanin loss of the crossbar architecture suggests that high optical power (a few mW per pixel) would be required. Thus the transition from off to on states due to absorbed radiation would occur rapidly, dictating a refresh rate dependent upon the maximum optical power incident on a pixel.

Operation in a two-wavelength scheme, using a wavelength close to the bandgap to set the weights, and a longer wavelength for communication, would increase the usable time between refreshes. The viability of this approach would depend upon the attainable extinction ratio for wavelengths corresponding to photon energies significantly below the bandgap.

2. Incoherent-to-coherent converters

In many optical signal processing architectures, coherent representation of a signal is required. Data presented to the system however may be in incoherent form. An example might be an imaged scene in which a given target was to be sought. The phase-based optical correlator requires that the signal be in coherent form. Optical addressing of spatial light modulators has been accomplished by integration of a photoconductive medium with a non photosensitive modulator. This has been used, for example, to demonstrate optically addressed ferroelectric liquid crystal modulators.

System requirements are for speeds of the order of kHz, and with high extinction ratios. Sensitivity to the incident radiation is an obvious prerequisite. For certain wavelengths of incident radiation, nipi structures may find application. Figure 2 shows a proposed scheme. Incident radiation below the bandgap serves to excite carriers in the nipi. For a wavelength of light just above the bandgap, the transmission will be modified. A filter eliminates the transmitted incoherent light, thus the incoherent input is converted to a coherent output. Electrical resetting of the nipis would be required to

4

refresh the input. Time taken for modification of the transmission state of the modulators would depend on the intensity, and some control over the exposure time would be required to prevent all pixels attaining their saturated transmission values.

3. Neural Networks

The term neural network is generally understood to encompass a wide range of architectures, characteristic of which are large numbers of highly interconnected processing elements of relatively simple functionality, and the ability to adapt either on-line or off-line to new information concerning the desired behavior of the system. The systems are, to varying extents, robust to imprecise data. A large number of models have been proposed, and for a full description of the current state of the art, the reader is referred to reference 6. The requirements on functionality of the components involved are easily understood by reference to a single-layer model (13). An optoelectronic implementation of a single-layer feed-forward model might consist of a (1 x N) linear input vector, expanded anamorphically to overlap an (N x N) weight matrix. The transmitted amplitudes across each row might then be summed. Critical to the implementation of many neural network models is a non-linear thresholding of the summed signals to provide the output from the single stage. Multilayer networks may be produced by using the output from the first layer as an input to a subsequent layer.
the system may be operated as an associative memory. A number of patters are stored (superimposed) on the weight matrix array. A given input will produce an output which represents the best matched of the stored patterns. Subsequent passes through the system serve to refine the output pattern, until it is a perfect recall of one of the stored vectors. Such a system has many uses, including reconstruction of complete data sets from partial representations, extraction of one of a set of known patterns from a noisy signal, and feature extraction from images.

In such an architecture, the input vector must be capable of being changed as rapidly as possible, since many iterations may be required to achieve convergence. The weight matrix is required to maintain constant weights during the recall mode, and should therefore have as long a lifetime as possible. During o-line learning, if supported by the system, the weight matrix elements must respond to required changes in transmissions. It is in the weight matrix that nipi SLMs may offer advantages over other approaches. It is likely that the device would be operated somewhat below bandgap in the pass-through mode, with optical addressing during the learning mode used to update the matrix elements. A hybrid system incorporating FLC input vectors and nipi weight matrix elements would be a strong contender. Provision for rapid reset of the SLMs via shorting of contact electrodes would be an important feature.

The possibility of non-linear variation in transmission with incident intensity would allow the use of NiPis as the output vector of a given stage in a multilayer architecture. Obviously, some control over exposure would be required, possibly using a liquid crystal shutter at the input to the entire system.

The field of neural networks is a rapidly expanding one, many new models evolving as the technology develops. The applications of NiPis to implementation of these models is outside the scope of this report, and should be further investigated.

4. Correlators

Optical correlators are of interest for pattern recognition (8), determining whether

5

an input image corresponds to a stored image within the correlator. The input to the correlator may be in the form of an optical signal, or an electrical signal derived from a sensor or sensor array. One commonly used architecture is the Van der Lugt correlator. In this architecture, the Fourier transform of an image field is obtained, and multiplied in some form by a filter in the Fourier transform plane (7). Appropriate signal processing is used to determine whether the value of the output is sufficient to pronounce the correlation positive. Shift invariance is provided by the use of the transform, in other words recognition of a target does not depend upon its location within the input field. Spatial light modulators find applications at both the input plane and the filter plane. Representation of the input information may be made by phase or by amplitude, as may the filter information. However, the correlator performance is severely affected by the choice of representation.

Information representation in Van der Lugt Correlators

The original architecture proposed by Van der Lugt enabled detection of a particular target in the image field by the use of a matched filter at the correlation plane. Since representation in the Fourier transform plane of an arbitrary object would require both phase and amplitude representations, such a combination of filters was constructed. Such filters however are complicated to fabricate, and other authors sought more cost effective solutions.

Horner (9) proposed a correlator in which the amplitude information is ignored, and a filter implementing only phase modulation across the field is used. In reference 9, the performance of phase-only, amplitude only, and full filters are compared. The analysis shows that amplitude only filtering is poorer in detecting a correlation than the matched filter, whereas the phase only filter has a sharper correlation peak and greater efficiency, at the expense of some reduction in the output signal-to-noise ratio. The highest signal-to-node ratio is always obtained for the full matched filter. Thus, if simple filters are to be fabricated, they should be of the phase-only variety. The reduction of signal-to-noise ratio compared to the matched filter may be justified if low light levels are present.

The refresh rate of the filter depends on the system application. Two general modes of operation exist. In the first, a range of filters are presented to the system in order that a given input may be classified. Having obtained classification of the signal, tracking may be require. Information derived from the tracking process may include a determination of whether a target is becoming closer or more distant, or other time-dependent information. In many systems, the filter values would remain constant during the second phase.

We now turn our attention to the input plane. The purpose of such a plane may be to convert an incoherent optical image to a coherent one, to convert the wavelength of an optical signal into one appropriate for the correlator, or to represent some non-optical information as an optical signal. The representation would be by amplitude, thus different categories of spatial light modulator from those applicable to the filter plane might be used. Requirements include a frame refresh rate adequate to detect changes in the target within a minimum acceptable period.

Having determined that the optimum representation of the filter information would be by a phase, or phase-plus-amplitude filter, and that an amplitude filter would be most appropriate for the input plane, several options exist for the range of allowable values

6

represented at each plane. The values may be analogue, two-valued, or binary with a higher level of resolution. The light used within the correlator may be coherent or incoherent. Coherent illumination is required for phase-based systems.

Binary representation If the device representing either the input image or the matched filter may assume only one of two states (-1/+1 or 0,1 for bipolar and unipolar devices respectively), and the image to be input is in binary form, then correct operation of the system will follow. This is of importance for NiPi devices used to fabricate high Q structures. Kumar has shown that if the image is not inherently binary, but has not been contaminated with noise, then the performance of the correlator will not be degraded. Psaltis (7) has investigated the effect of thresholding on an input which has been corrupted by additive random noise. The performance of the correlator is actually improved if the input signal to noise ratio is poor (2.0 for example), while for high SNR inputs, the output SNR is not appreciably degraded.

In a single pass through the thickness of an SLM of thickness 10 microns, an index change of 0.04 would be required to achieve a 180 degree phase change. On the assumption that this is infeasible for the nipis without an associated change in absorption, we will not consider the possibility of phase-only filtering, and consider only amplitude modulation based correlators.

Two modes of operation are commonly cited. In the first, target recognition, a number of matched filters are provided to the system in order that the best fit to the presented data may be determined. In the second, a recognized target is tracked, with only a single filter being used. Issues of concern in implementing the Van der Lugt correlator are the speed at which successive images are updated, and the speed at which different target filters may be presented if more than one match is to be determined. Use of the nipis as SLMs would require an offset in the output if bipolar values were to be represented, since only unipolar representation may be performed with the modulators. Reported implementations have used many types of modulator including magnetooptic modulators. If the signal to be investigated arrives in electrical form, access to the modulators is required to impress the information on the light. For increasingly large input arrays, it will become infeasible to provide a single interconnection for each pixel. The Litton magnetooptic device (MOD) arrays use sequential access to each pixel via the intersection of horizontal and vertical electrical lines. Thus the total frame rate is given by the speed of each pixel divided by the total number of pixels. Thus for an array of size 50 x 50, a millisecond frame rate would require a device speed of 0.4 microseconds, and would also require that the modulators be able to retain their allocated transfer functions for one millisecond, while being able to relinquish control in less than 0.4 microseconds.

In the case of optically input data, the SLM input array would function as an incoherent-to-coherent converter.

5) Displays

For application to displays, requirements placed on a spatial light modulator are that it have a speed comparable to the minimum time required to refresh the display. Frame

7

refresh rates of 1kHz are ample for most applications. At this speed, many SLMs are appropriate. The choice of material is governed primarily by drive voltage, operating wavelength, and contrast ratio. The application o nipis to displays seems doubtful, since the change in absorption from excited to unexcited states is most significant at the bandgap. Display applications are associated with electrical addressing, thus the requirement for high intensities for displays would not result in rapid absorption and conversion from off to on states for the modulator if pixels to be in the off state were shorted.

6) Spectrum analysis

Effron (1) has described a system in which high bandwidth spectrum analysis is performed in real time. The signal to be analyzed is applied to a CRT, and the information displayed thereon is transferred to an optically addressed spatial light modulator. The modulator then behaves as an incoherent to coherent converter, and the fourier transform of the signal obtained. The application of nipi SLMs to this system would be limited by the sensitivity of the device to the radiation emitted by the CRT, and by the erase time in order that successive sweeps of the CRT do not result in several samples of the signal being superimposed on the SLM. nipis are not expected to be suitable for this application.

7) Optical and Optoelectronic Logic

The property of variation in some optical characteristic with optical intensity of any device would suggest that the application to optical logic be considered. Whereas neural networks are analogue architectures, much effort in optical computing is focussed on optical equivalents of digital electronic computers. Before such systems can be realized in a manner offering any improvement over optics, critical elements such as addressable optical memory must be developed. Assuming the ultimate existence of such components, higher throughput compared to electronic computers may be realized only if logic functions may be performed in substantially shorter times (speeds of tens of gigahertz being sought), or if substantial parallelism can be introduced. Given the speed at which the nipis excited carriers could be removed, it seems doubtful that high throughput could be sustained in a system incorporating them, if modification of optical transmission via photoexcitation is the non-linear mechanism. If the instantaneous non-linear properties of the material are to be used, the non-linear coefficients of the material are the critical parameter, and must be compared against those of the many competing materials.

Conclusion

The requirements placed on SLMs in a range of optical systems have been considered, and the potential performance of nipi based devices compared to the performance attainable using other SLMs. In general, the nipi devices are poor choices for electrically addressed SLMs due to their low speed. As optically addressed SLMs however, the nipis may have higher sensitivity than other optically addressed SLMs, rendering them useful for incoherent-to-coherent converters. These would in turn find

application in correlators, primarily at the input plane. The potential of non-linear transfer functions also indicates that the nipis may find applications in optoelectronic and all-optical implementations of some neural network models. The use of NiPis in optical interconnects opens up some new possibilities for optical configuration of crossbars, however the poor scalablity of masking-type crossbars will limit the application of the devices to extremely small systems.

References

1) Efron,U, "Spatial Light Modulators for Optical Information Processing", Proc. SPIE, Vol 700 IOCC, 1986, pp132-145

2) G.Moddel, C.T.Kuo, K.M.Johnson, W.Li, "Optical Addressing of High-Speed Spatial Light Modulators with Hydrogenated Amorphous Silicon", Proc. Materials Research Symposium, Vol 118, 1988, pp405-410

3) D.Armitage, J.Thackara, W.Eades, "Ferroelectric Liquid Crystal Devices and Optical Processing", Ferroelectrics, Vol 85, pp291-302

4) C.Land, "Optical Information Storage and Spatial Light Modulation in PLZT Ceramics", Optical Engineering, Vol 17, No 4, 1978, pp317-326

5) T.Minemoto, S.Numata, and K.Miyamoto, "Optical Parallel Logic Gate using Light Modulators with the Pockels Effect: Applications to Fundamantal Components for Optical Digital Computing", Applied Optics, Vol 25, No 22, 1986 pp4046-4052.

6) DARPA Neural Network Study, AFCEA Press, 1988

7) D.Psaltis, E.Paek, S.Venkatesh, "Optical Image Correlation with a Binary Spatial Light Modulator", Optical Engineering, Vol 23, No 6, 1984, pp698-704

8) M.Giles, J.Taylor, N.Grijalva, and B.Gioannini, "Optical Image Correlation Using a Deformable Mirror Device: A Feasibility Study", Proc. SPIE, Vol 753, 1987, pp72-81

9) J.Horner, P.Gianino "Phase-Only Matched Filtering", Applied Optics, Vol 23, No. 6, 1984, pp812-816

10) Huignard,J.P, "Spatial Light Modulators and Their Apr   ations", Proc. International Topical Meeting on Image Detection and Quality, 1986, pp291-301

11) T. Minemoto, S.Numata, K.Miyamoto, "Optical Parallel Logic Gate using Spatial Light Modulators with the Pockels Effect: Implementation using three PROM Devices", Applied Optics, Vol 25, No 6, 1986, pp948-955

12) Recording Phase Deformations on a PLZT Wafer for Holographic and Spatial Light

Modulator Applications", Proc. SPIE, Vol 551, 1985, pp96-100

13) Hopfield, J.J, "Neural Networks and Physical Systems with Emergent Collective Computational Capabilities", Proceedings of the National Academy of Sciences, Vol 79, 1982, pp2554-2558
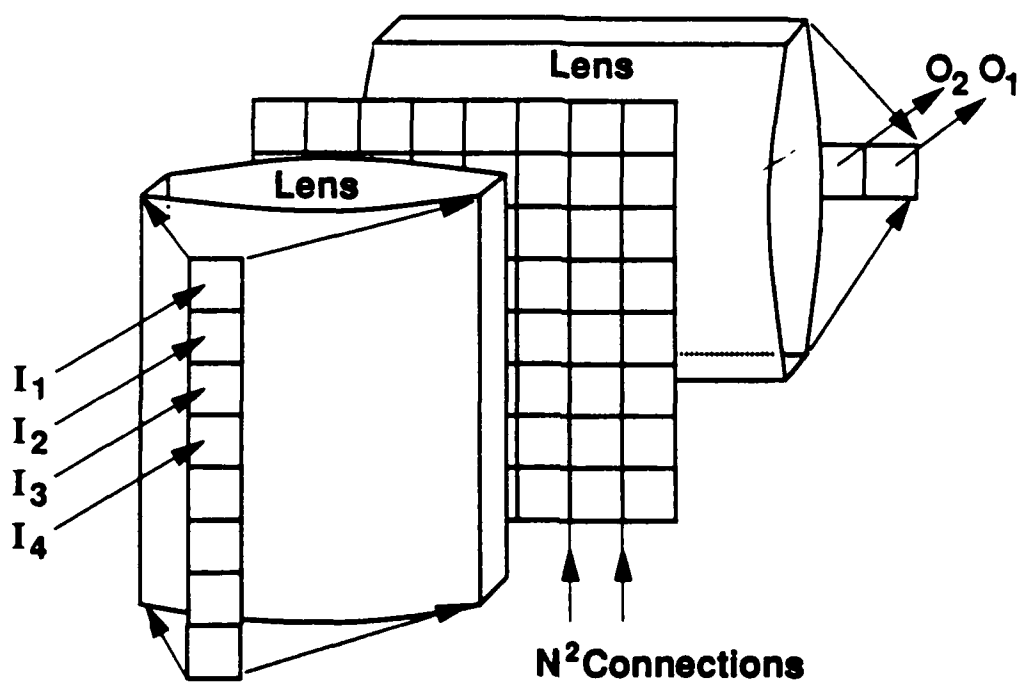
Figure 1. Illustrating the Use of Spatial Light Modulators for Interconnection
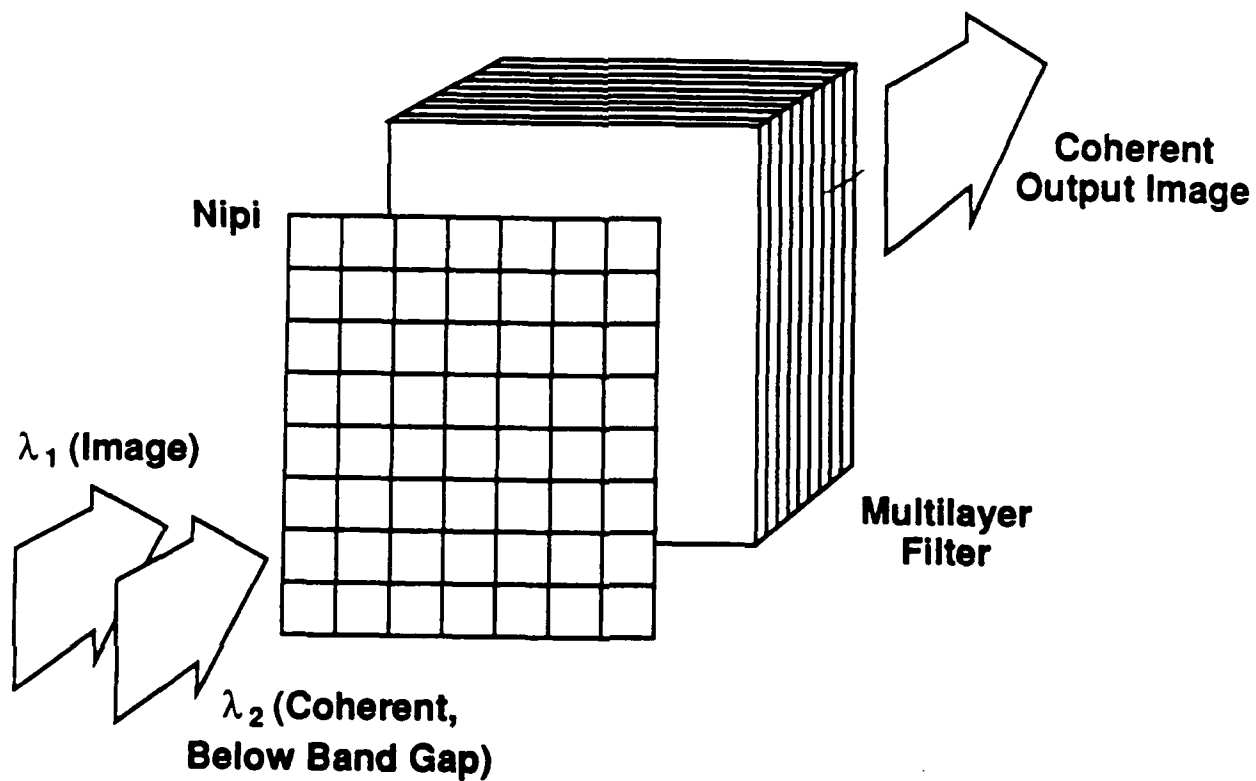
Figure 2. Transmissive Nipi Based Incoherent-to-Coherent Converter.